Bull. Astr. Soc. India (1984) 12, 109-151

The Be star phenomena
II. Spectral formation and structure of envelopes

Ryuko Hirata and Tomokazu Kogure
Department of Astronomy, Faculty of Science, University of Kyoto, Kyoto 606, Japan

Received 1983 September 19

Abstract. In succession to the general considerations in Paper I, a review of the spectral formation and the structure of envelopes are presented.

An overall theoretical discussion of the envelope dynamics and the radiation field as the basic processes in the cool envelopes of Be stars is first given.

The formation of continuous spectrum is considered in terms of the volume emission measure and the optical thickness in the continuum. As for the emission lines, it is shown that the emission equivalent width of the Hα line, Wα, and the Balmer decrement Hα/Hβ, as the spectral-type dependence, can be qualitatively explained by both the static- and moving-envelope approaches, provided the constant optical thickness of envelopes in the Lyman continuum along the spectral sequence of Be stars. Paschen decrement Pn/P14 (n = 11–24) can be explained if the envelopes are optically thin for the Paschen lines higher than about n = 15. The peak separation v_P of the double-peaked emission profiles is given as a good indicator of the outer equatorial radius of envelopes. The significance of the (Hα/Hβ — $W\alpha$) diagram is emphasized as a tool for the diagnostics of cool envelopes.

In the analysis of shell absorption lines, the curve-of-growth method and the central-depth method are presented with some critical arguments. A possibility of explaining the Balmer progression by pure absorption process is pointed out.

Importance of the diagnostics of envelope structure is emphasized. Some arguments on the flatness, detachedness, elongation, inhomogeneity, and velocity field are presented from this point of view.

Finally the structure and origin of hot regions are briefly reviewed with particular attention to the geometrical relationship between cool and hot envelopes. Supporting arguments for the bidimensional arrangement consisting of a cool equatorial disc and a hot spherical region are given.

Key words : Be stars—shell stars—continuous spectrum—emission lines—shell absorption lines—cool envelopes—hot regions

1. Introduction

In Paper I (Kogure & Hirata 1982) we reviewed Be stars and Be-star phenomena, mainly on the basis of their statistical properties. It has been shown that there is no essential difference in stellar parameters between B and Be stars except in the average rotational velocities and in the formation of cool envelopes around the stars. Thus the study of Be-star phenomena is principally directed towards obtaining an understanding of cool envelopes in their structure, origin, stabilities, and of their relationship to the hot expanding regions which are observable both in B and Be stars.

In this paper we begin with a brief review of the envelope dynamics and radiation field as the basic processes in the cool envelopes of Be stars. Then we proceed to discuss the spectral formation of the continuum radiation, emission lines and shell absorption lines. Comparison between observations and theories has been made for some of these spectral features. In the next part we consider the structure of cool envelopes and hot expanding regions. Importance of diagnostics for the structure of cool envelopes is emphasized, though the methods are not yet fully developed. Our considerations are mainly focused to pick up star candidates having special behaviour of cool envelopes in their flatness, detachedness, elongation, inhomogeneity, and internal velocity field. For the hot regions the relationship between cool envelopes and hot expanding regions in the geometrical and physical structure will be briefly considered.

2. Basic physical processes

The study of Be star phenomena principally aims at understanding cool envelopes in the radiation process as the origin of spectral features and in the dynamical process by which the envelopes are formed and maintained. In both processes the rapid rotation of central stars may have important effects. In this section we give an overall insight into these problems from a theoretical point of view.

2.1. Be stars as rapidly rotating stars

Rapid rotation is a basic characteristic of Be stars. If a rotating star is in hydrostatic and radiative equilibrium, then the total flux $\pi F(= \sigma T_{\rm eff}^4)$ must be proportional to the local effective gravity $g_{\rm eff}$ (von Zeipel 1924). This means that the effective temperature $T_{\rm eff}$ decreases from star's pole to its equator in a rotating star. This is the so-called rotationally induced gravity-darkening and it may affect observational behaviour of Be stars and other rapidly rotating stars.

Collins & Sonneborn (1977), in their extensive calculations of model atmospheres, have suggested that the rapid rotation pushes a main-sequence star up in its colour-magnitude diagram. Slettebak *et al.* (1980), on the basis of same model atmospheres and calculation of absorption lines, have found that the spectral type of rapid rotator seen equator-on shows a shift to later type as compared with non-rotating stars, supporting the above conclusion.

The effect of gravity darkening becomes more apparent when we compare the ultraviolet and visible regions, since the difference of effective temperature gives rise to different spectral behaviour in both regions. Kodaira & Hoekstra (1979)

made a comparison of continuous spectra for pole-on stars. Heap (1976) found that in the case of ζ Tau the photospheric lines are narrower in the ultraviolet region than in the visible region by a factor of two or three in velocity unit.

Heap's result has stimulated theoretical considerations of Hutchings (1976), Sonneborn & Collins (1977), Collins & Sonneborn (1977), Hutchings *et al.* (1979), and Ruusalepp (1982). If the ultraviolet lines are formed in hot polar regions, the difference in line widths of ultraviolet and visible lines makes possible, in principle, to separate the equatorial rotation velocity V_* and the inclination angle i from observed value of V_* sin i in two spectral regions. Hutchings *et al.* (1979) and Ruusalepp (1982) have made their effort along this line. However, as pointed out by Marlborough (1982), the procedure depends upon the adopted models and underlying assumptions, so that it is still difficult to reliably separate the values of V_* and i. In view of the importance of this separation in the study of Be stars, further development both in observation and theory will be highly appreciated.

Concerning the origin of Be stars, Sackmann & Anand (1970), Endal & Sofia (1979) and Endal (1982) have investigated the effect of the evolution of rapidly rotating stars. According to them, stars rotating faster than 50% and 70% of ZAMS critical velocity for 10 and 5 $M_\odot$ stars respectively, can reach the critical rotation before reaching the state of hydrogen exhausion. According to Endal (1982) the statistics of Be-star frequency does not contradict this theoretical prediction. It is, however, to be mentioned that the critical rotation is not a condition for a star to be a Be star. Actually most of Be stars are rotating much slower than their critical velocities, especially early-type Be stars (section 4 of Paper I). Late-type Be stars are rotating faster, and are nearer critical velocities, so that appreciable effects of gravity darkening and of stellar evolution could be expected in these stars.

2.2. Envelope dynamics

The physical parameters which regulate the dynamical state of Be envelopes include rotation, radiation pressure, magnetic field, non-radiative heating, and probably inflow of matter in case of binary systems. The evaluation of these factors is a basic procedure toward the understanding of envelope dynamics.

From the dynamical point of view, the most outstanding feature is the equatorial extension of cool and dense gas over several stellar radii, as will be shown later (section 6). The concept of plane-parallel stellar atmospheres in hydrostatic equilibrium obviously breaks down for such extended envelopes. It is then inevitable to introduce some additional pressure forces (direct support), or effective reduction of gravity by centrifugal force over the whole envelope (centrifugal support).

Historically, Limber (1964) first investigated the hydrostatic configuration of rotating envelopes, according to which a temperature of a few or ten million Kelvin is required for supporting the envelope. This situation remained unaltered when rotationally-forced stellar wind was introduced (Limber 1967). In this case, though the critical sonic point of stellar wind is located at a radius well separated from the star ($\sim 10\ R_*$), the existing steep velocity gradient in the subsonic region severely reduces the gas density and confines the envelope to a small extension. The inclusion of radiation pressure (Marlborough & Zamir 1975) could not change

the situation. After a survey of supporting mechanisms, Limber & Marlborough (1968) concluded that the most probable one is the centrifugal support maintained by either magnetic or turbulent viscosity.

An alternative view of direct support in a rapidly rotating star with magnetic field has been advocated by Morozov (1973), Saito (1974) and Limber (1974), as an extension of Weber-Davis' (1967) formalism. In these models we can see several aspects of behaviour favourable to the situation of Be envelopes : (a) Low gradient of radial velocity, which is visualized due to essentially azimuthal configuration of magnetic field, allows a large extension of envelopes, along with low terminal velocity. (b) The break-up velocity of stellar rotation is not a necessary condition. (c) The strength of magnetic field required is less than a few hundred Gauss at the bottom, which is below the upper limit of present-day observations (Landstreet 1980; Scholz 1981). In this case the circular velocity is essentially given by the law of angular momentum conservation ($v_\phi \propto 1/r$) except in the innermost part of the envelope. Barker (1982) has found that the circular velocity is reduced even below the $1/r$ law in the inner part of envelope when steep acceleration due to radiation pressure is introduced.

Weber-Davis formalism has been further discussed by Nerney (1980), Barker & Marlborough (1982); and a time-dependent model has been investigated by M. Saito & Y. Saito (1983, personal communication) in an attempt to explain Pleione's shell episode. According to a current view, it is the magnetohydrodynamical model of stellar wind that most favourably reproduces the dense and extended envelopes around Be stars on a suitable scale.

Concerning the vertical structure of envelopes, Limber (1967) and Křiž (1979a) suggested a hydrostatic configuration, according to which the envelope is confined near the equatorial plane of the star. In actual cases, Be envelopes reveal a large variety in their vertical extension (see section 6). This means that the hydrostatic condition is often violated for some reasons. One possible reason is that the area of mass-ejecting region on the stellar photosphere extends up to a certain latitude in both sides of star's equator.

The binary hypothesis provides a different picture for the envelope dynamics (Harmanec 1982). Inflowing gas from the secondary brings mass and excess angular momentum, making an accretion disc or ring around the primary B star, where the circular velocity is Keplerian. Křiž (1982) has considered the physical processes in the accretion discs, along with the fate of excess angular momentum. The binary hypothesis is very attractive at least for some Be stars. Although the relationship between single-star origin and binary interaction is not clear at present, it is highly desirable to develop the hydrodynamical simulation for well-known binary systems.

2.3. Radiation field

An envelope of Be star, which is relatively cool and exposed to strong ultraviolet radiation of the central star, has two distinct optical properties in general. First, it is rather optically thin for the continuous radiation in the visible region, as we can see the stellar line spectrum through the envelope. Second, it is optically thick for the hydrogen Balmer lines. because strong shell absorption lines are observable in

shell stars and observed Balmer decrements exhibit a large variation from star to star and from time to time.

These two properties characterize the radiation field of Be envelopes as an intermediate type between stellar photospheres which are essentially in LTE and planetary nebulae. In the latter, the so-called Rosseland cycle is effectively operating, *i.e.*, the photoionization from the ground state by stellar ultraviolet radiation is followed by recombinations and subsequent cascade transitions to form a pure emission-line spectrum. In contrast, the Be-type radiation field is basically characterized by the importance of photoionization from the second energy level of hydrogen atoms, as first suggested by Sobolev (1947) and Miyamoto (1949). The intermediate character of the Be-type radiation field may be roughly seen in table 1.

Table 1. Comparison of radiation fields

Typical field	Stellar photosphere	Be-envelope	Planetary nebula
Gas density (cm^{-3})	10^{13}–10^{15}	10^{10}–10^{12}	10^{3}–10^{5}
Dilution factor	~ 1	10^{-1}–10^{-3}	10^{-14}–10^{-16}
Deviation from LTE	Nearly LTE	Non-LTE Incomplete Rosseland cycle	Non-LTE Effective Rosseland cycle

The theory of radiation field of Be envelopes has been developed historically by two methods of approach, *i.e.*, static and moving-envelope approaches.

In the static approach the equations of radiative transfer are coupled with the equations of statistical equilibrium for atomic level populations, and solved under the situation of no velocity gradient. The three-level problem for hydrogen atoms was first solved by Miyamoto (1949) and 4- to 7-level problems by Miyamoto (1952a, b), Kogure (1959a, b, 1961, 1967) and Pottasch (1961). The difference between Miyamoto's and Kogure's treatments lies in the assumption of optical thickness for the Paschen and higher series of hydrogen, *i.e.*, optically thick in Miyamoto's and transparent in Kogure's treatment. Pottasch (1961) has added the effect of collisional transition processes. All have calculated the Balmer decrement Hα/Hβ as a function of the geometrical dilution factor W. Typical cases of their calculations are shown in figure 1. One may notice that the theoretical decrement sensitively depends on the assumption of line opaqueness and the effect of collisional processes. Kogure (1969a) has applied his method to the calculation of Hβ emission profiles of Be stars, by dividing the envelope into a suitable number of equal line-of-sight velocity zones.

The second approach is the method of moving envelope, originally proposed by Sobolev (1947) and developed by many authors (see Briot 1981a; Kříž 1973). In this method the solution of transfer problem is practically replaced by the calculations of photon escape probabilities due to existing velocity gradient. Inserting the calculated probabilities into the equations of statistical equilibrium for a sufficient number of energy levels, we can calculate the emission line intensities and line profiles. Application to the Be envelopes has been made by Doazan (1965), Lacoarret (1965), and, recently by Kříž (1979a, b). Briot (1981a) has examined the

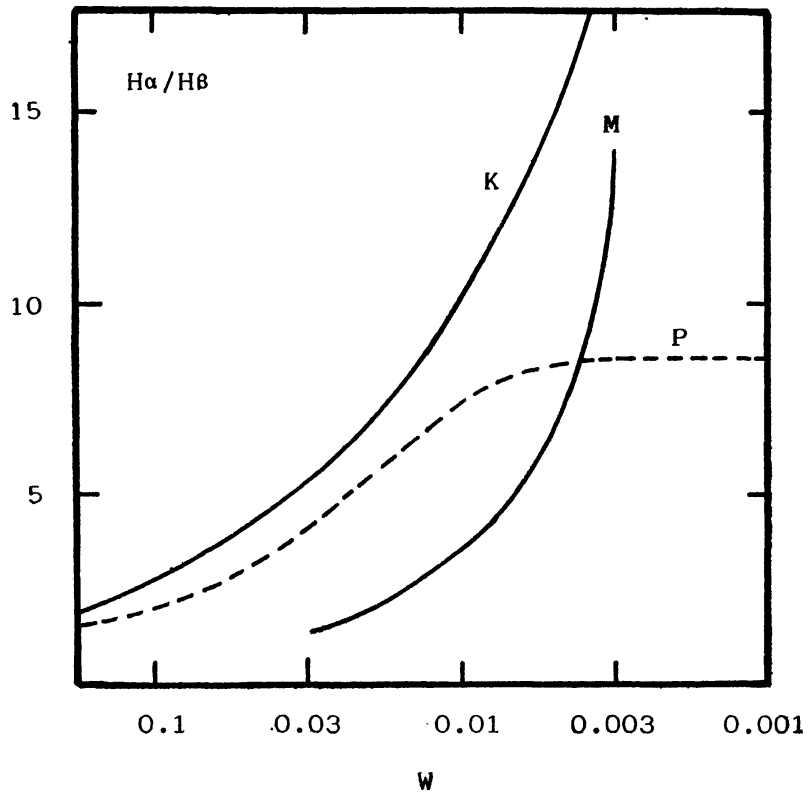

Figure 1. Balmer decrement Hα/Hβ as function of the dilution factor W calculated in the static envelope approach. The curves designated by M, K, P indicate the cases of Miyamoto (1952), Kogure (1959b, case V), and Pottasch (1961), respectively. The temperature is $T = 20{,}000$ K in all cases and the electron density is $N_e = 10^{11}$ cm^{-3} in case of Pottasch (1961).

relative intensities of the Paschen and Balmer emission lines and pointed out some problems (section 4.2).

Recent extensive model calculations of Poeckert & Marlborough (1978a, b) are based on the method of Marlborough (1969, 1970), which essentially uses the static approach. Based on modified nebular radiation fields, this method takes into account the line opaqueness in the form of optical depth perpendicular to the equatorial plane, thus without solving the equations of radiative transfer.

Finally we show the values of b_n, the deviation factor from LTE for the nth energy level, as functions of the radial distance from the central star, in order to see the characteristic feature of radiation field over an entire region of Be envelope. In figure 2 the theoretical values of b_n ($n = 1, 2, 3, 4$), calculated by Poeckert & Marlborough (1978a) and Kříž (1979b) are shown. The adopted envelope parameters are

$$T_e = 20{,}000 \text{ K}, \quad N_{e,0} = 3.33 \times 10^{13} \text{ cm}^{-3}$$

(Poeckert & Marlborough 1978a)

and

$$T_e = 20{,}000 \text{ K}, \quad N_e = 1 \times 10^{10} \text{ cm}^{-3} (= \text{const})$$

(Kříž 1979b),

where $N_{e,0}$ indicates the electron density at the stellar surface. The former treats denser envelopes than the latter. In figure 2 broken line gives $b_2 = 1/W$, which an

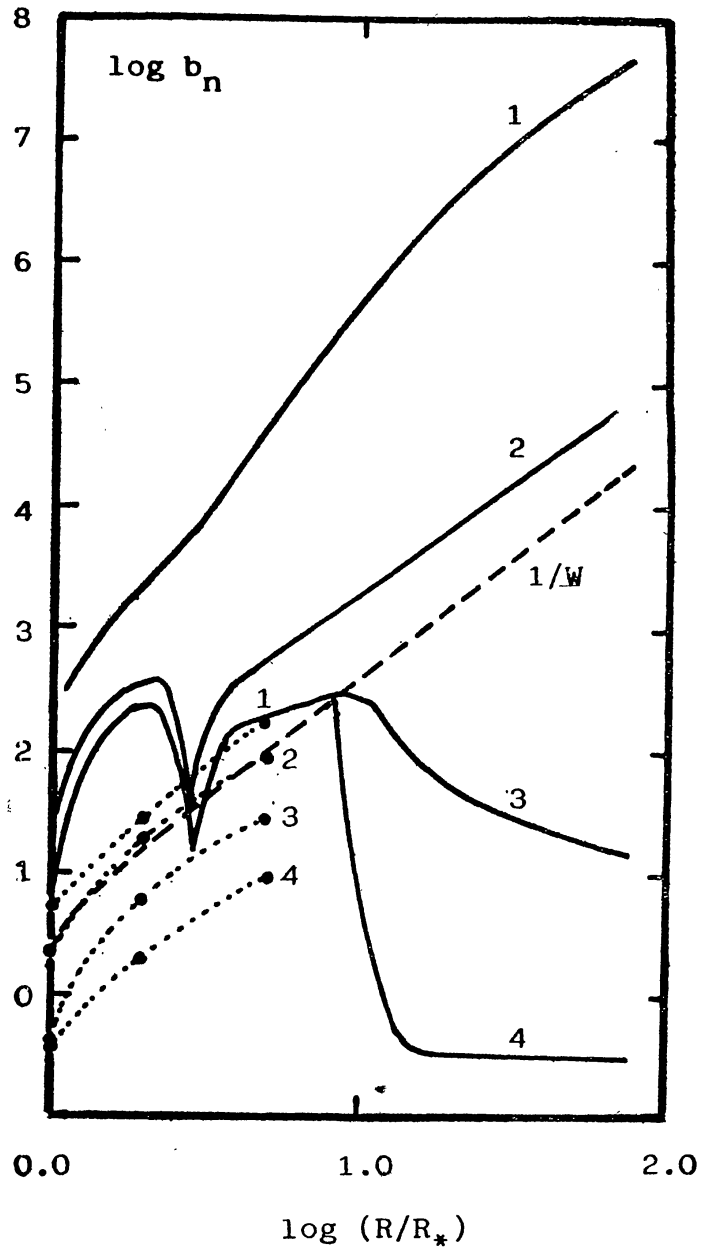

Figure 2. The deviation factor $b_n(n = 1, 2, 3$ and $4)$ of hydrogen atom in recent model calculations. The values in the equatorial plane are shown as a function of distance $r = R/R_*$. The n value is indicated in each line. Solid line represents the result of Poeckert & Marlborough (1978a). The dotted line shows the result of Kříž (1979b). The broken line correponds to $1/W$, where W is the dilution factor.

essential result of Miyamoto (1949). We also notice that b_1 is given by $b_1 \sim e^{\tau}/W$ in the frame of modified Saha equation (Sobolev 1947), where τ denotes the optical depth in the Lyman continuum. General coincidence of b_n-factors with the $1/W$ law in the inner part of envelopes may be apparent, whereas the values of b_3 and b_4 decrease in the outer region, tending toward those of planetary-nebula solution (Poeckert & Marlborough 1978a). Optically thin nature of the outer region may bear the decrease of b_3 and b_4.

From these calculations we can conclude that the radiation field in Be envelopes consists of two parts: the inner field which is typical of Be-type radiation field and the outer field which is essentially the nebular type field. Practically the outer field has no effect on the formation of emission lines and continuum because of low gas density in the outer regions.

3. Continuum radiation

3.1. Summary of observational behaviour

We first summarize the general properties of observed continuum radiation of Be stars which are to be interpreted consistently by the existence of cool envelopes.

(i) Infrared excess is often detected (*e.g.* Allen 1973; Gehrz *et al.* 1974; Schild 1976; Feinstein 1982), in as many as 60% of Be stars (Mendoza 1982). There is a tendency that infrared excess is higher when Hα-emission is stronger (Neto & Pacheco 1982; Feinstein 1982), and strong infrared excess is accompanied by the Paschen lines in emission (Briot 1977). The near-infrared excess of Be stars has two main types: one can be explained by optically thin free-free radiation from cool envelopes, and the other is due to re-radiation from circumstellar dust (Allen 1973). The latter case is mostly detected in the late-type Be to Ae stars. When infrared excess is interpreted as free-free emission, the envelope is often optically thick in the spectral region of $\lambda \gtrsim 8$ μm (Gehrz *et al.* 1974).

(ii) A large fraction of Be stars exhibits brightness variations with a typical amplitude of $0^m.1$–$0^m.4$ (Feinstein 1968, 1975; Feinstein & Marraco 1979). In early-type Be stars, the brightening in V band is usually accompanied by the reddening in $B-V$ colour. Late-type Be stars with large values of $V_* \sin i$ exhibit just inverse correlation (Nordh & Olofsson 1977; Hirata 1982a; Hirata & Hubert-Delplace 1981). Parallel and anti-parallel relations are both found between brightness and E/C variations (section 8 of Paper I).

(iii) Intrinsic linear polarization up to 2% is a general characteristic of Be stars. Between polarization degrees and rotational velocities there is an apparent correlation in the sense that Be stars with larger values of $V_* \sin i$ can reach higher polarization degree (see section 6). A marked behaviour of linear polarization is its strong wavelength dependence, *i.e.* the polarization degree increases with decreasing wavelength toward the hydrogen series limits (*e.g.* Coyne 1976; Poeckert *et al.* 1979; Jones 1979).

(iv) The ultraviolet flux of Be stars is generally deficient in the wavelength region λ 1650–2500 Å as compared with normal B stars (Beeckmans & Hubert-Delplacc 1980). Decrease of the ultraviolet flux has also been observed in the shell phase of some Be stars such as 59 Cyg (Beeckmans 1976) and 28 Tau (Golay & Mauron 1982).

(v) Thirteen-colour photometry by Alvarez & Schuster (1982) shows remarkable variations of energy distribution in the spectral region 0.33–1.1 μm. Figure 3 illustrates examples of such variation in three stars, X Per, HD 184279 and 28 Tau. X Per (Ope) has declined in brightness from 1977 to 1979. The minimum variation was observed at about 4000 Å, whereas larger amplitude variations occurred in the Balmer and Paschen continua, suggesting the predominant role of hydrogen

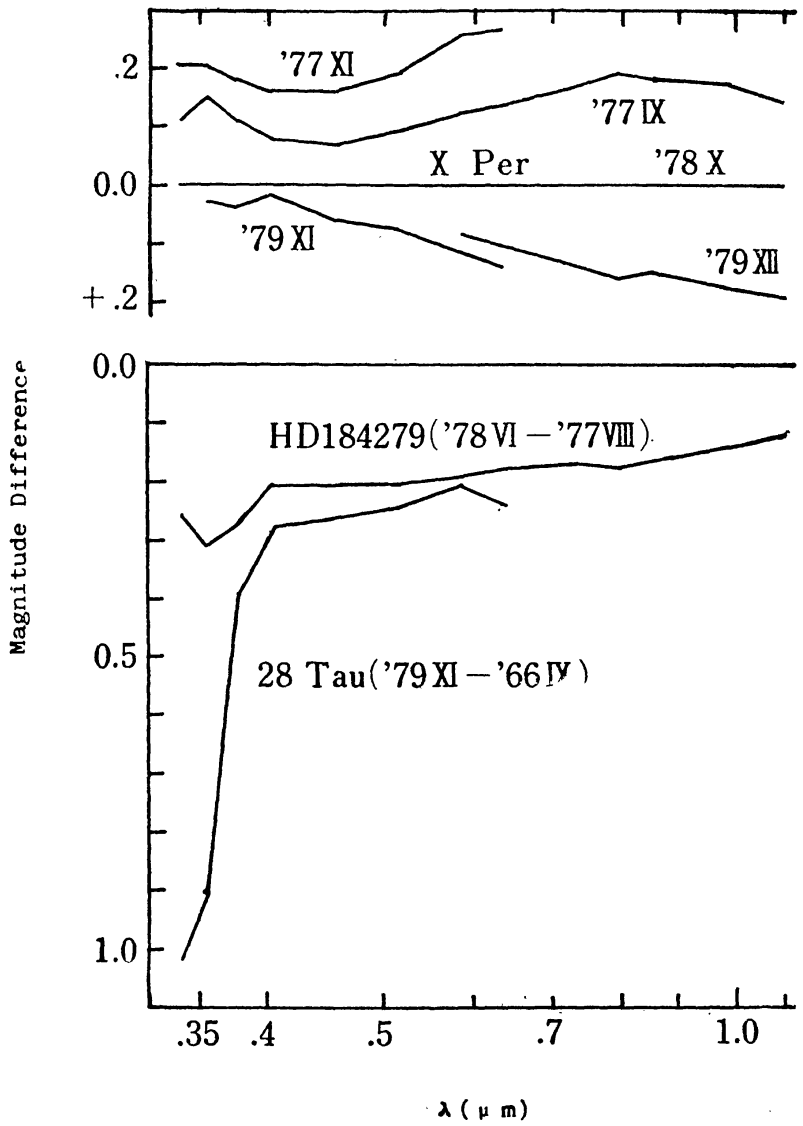

Figure 3. Variations of energy distribution in the 13-colour photometric system for three Be stars (Alvarez & Schuster 1982). Magnitude difference is expressed referring to the magnitude at the epochs of 1978 October for X Per, 1977 August for HD 184279, and 1966 September for 28 Tau.

bound-free radiation as emission or as absorption. HD 184279 (B0.5 IVe) has shown rather flat variation in 1977–1978 in the Paschen continuum. This implies that electron scattering is acting as a main source of opacity. Spectroscopic behaviour in these epochs is reported by Ballereau & Hubert-Delplace (1982). Finally, 28 Tau (B8 IV −Vpe) has shown a remarkable decrease of the Balmer continuum in shell phase (1979) from its pre-shell phase (1966), implying the effect of bound-free absorption in the Balmer continuum. Small amplitude variations and its wavelength dependence in the Paschen continuum are notable in HD184279 and in 28 Tau. This is in contrast with that in X Per.

3.2. Formation of continuous spectrum

We proceed to an interpretation of observed behaviour of continuous spectrum such as summarized in the previous section.

Sonneborn (1982), using his model atmospheres of rotating stars, confirmed the earlier conclusion (see Coyne 1976) that the observed linear polarization in Be stars does not originate from stellar photospheres. Then the most probable way is to attribute it to the electron scattering in non-spherical envelopes (see Coyne 1976). The observed wavelength dependence of polarization suggests the strong contribution of hydrogen recombination and/or bound-free absorption in the Balmer and Paschen continua. Time variations in the energy distribution such as displayed in figure 3 are also attributable to the combined effect of electron scattering and bound-free transitions. Although we have no sufficient observational data on the relationship in variations between polarization and brightness or other spectral features (*e.g.* Coyne & McLean 1982), it may be reasonable to suppose that the linear polarization and the continuous radiation are formed in the same non-spherical cool envelopes, which are also identical with the regions responsible for the formation of emission and shell absorption lines.

For simplicity let us assume an envelope of cool hydrogen plasma and examine its optical properties. When this plasma is isothermal and optically thin, the emitted energy distribution can be expressed by $\alpha\epsilon_\nu$, where ϵ_ν denotes the emissivity of free-free and free-bound radiatian per electron, and α the volume emission measure. The latter is defined by

$$\alpha = \int N_e^2 \, \mathrm{d}\, V/(\pi R_*^2),$$

where N_e denotes the electron number density, V the total volume of plasma, R_* the stellar radius. Then the product $\alpha\epsilon_\nu$ yields the energy distribution emitted from this plasma and expressed per unit stellar surface, *i.e.* the value of $\alpha\epsilon_\nu$ can be compared with stellar flux. Calculation has been made in two cases of $T_e = 10^4$ K and 2×10^4 K for hydrogen atoms with 10 discrete energy levels and for an adopted value of $\alpha = 10^{36}$. The results are shown in figure 4 in magnitude scale, together with stellar energy distribution F_ν^* and the blackbody radiation $B_\nu(T)$. The stellar energy distributions are taken from Kurucz (1979) for 3 sets of effective temperature with $\log g = 4.0$.

In figure 4 we can examine the relative contribution of stellar flux and envelope emission in a wide spectral region. In case of $\alpha = 10^{36}$, infrared excess appears in the region of $\lambda > 2 \sim 3\,\mu$m. In order that the envelope emission becomes appreciable in the Paschen continuum, the value of α must be larger than 10^{36}. Gehrz *et al.* (1974) obtained $\alpha = 10^{35} \sim 10^{36}$ from observed infrared excesses. If we adopt a disc model of constant vertical thickness of $\sim R_*$ and of average electron density of $N_e \sim 3 \times 10^{11}$, these values of α yield the equatorial outer radii of $2 \sim 6\, R_*$.

When the envelope is optically thick, we have to integrate the source function over whole envelope with a weight of exp $(-\tau_\nu)$, where τ_ν is the optical depth at frequency ν. If the envelope becomes completely opaque in all spectral region at its extreme end, then the envelope emission can be approximated by $B_\nu(T) \times S$, where S denotes the projected area of the envelope seen from the observer. In this case, as shown in figure 4, the contribution of envelope emission becomes remarkable, if the projected area S is comparable or larger than the stellar surface πR_*^2.

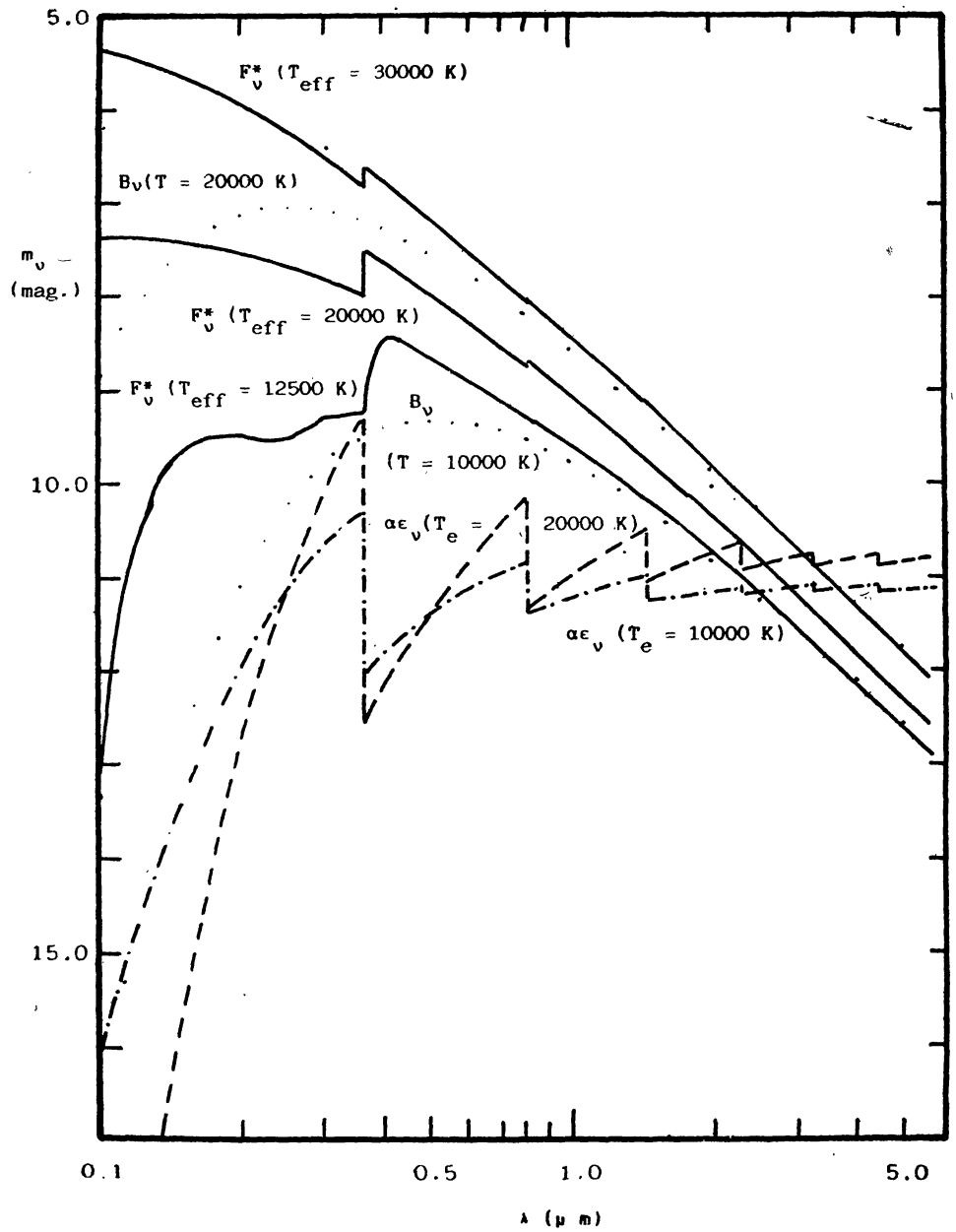

Figure 4. Comparison of the stellar flux and continuous emission of optically thin hydrogen plasma. Solid lines show stellar flux F_ν^* for $T_{eff} = 3 \times 10^4$, 2×10^4 and 1.25×10^4 K with $\log g = 4.0$. The broken and broken-dot lines represent the continuous emission from the optically thin hydrogen plasma, $\alpha\epsilon_\nu$, for $T_e = 2 \times 10^4$ and 10^4 K, respectively, where ϵ_ν is the emissivity per electron and α is the volume emission measure. The blackbody radiation, $B_\nu(T)$ for $T = 2 \times 10^4$ and 10^4 K (dotted line) is also shown.

Figure 4 also shows that the envelope emission contributes towards reddening the photospheric radiation and to decline the polarization degree toward longer wavelength in each spectral band between series limits. These trends are confirmed by observations.

In the next place, let us consider the absorption feature of an isothermal hydrogen plasma in LTE, adopting a typical case of $N_e \sim 3 \times 10^{11}$ cm^{-3}, $\tau_e \sim 0.1$ (the optical depth for electron scattering), $T_e = 10^4$ K and 2×10^4 K. These figures

give an effective geometrical thickness of 7.2 $R_\odot$, a typical value for a Be star. Figure 5 illustrates the wavelength dependence of the optical thicknesses for free-free (τ_{ff}) and bound-free (τ_{bf}) absorptions, besides τ_e. It is seen that $\tau_e \gtrsim \tau_{bf} \gtrsim \tau_{ff}$ for most of spectral range, and $\tau_{ff} \gtrsim \tau_{bf} \gtrsim \tau_e$ in the infrared region ($\lambda > 2 \sim 3\ \mu$m). Since $\tau_e \propto N_e$ and $\tau_{ff}, \tau_{bf} \propto N_e^2$, the rôle of bound-free and free-free absorptions increases with increasing electron density. These absorption processes destroy the polarized light and then act to decrease the polarization degree in the longer wavelength region. In addition, if these opacity sources diminish the starlight in

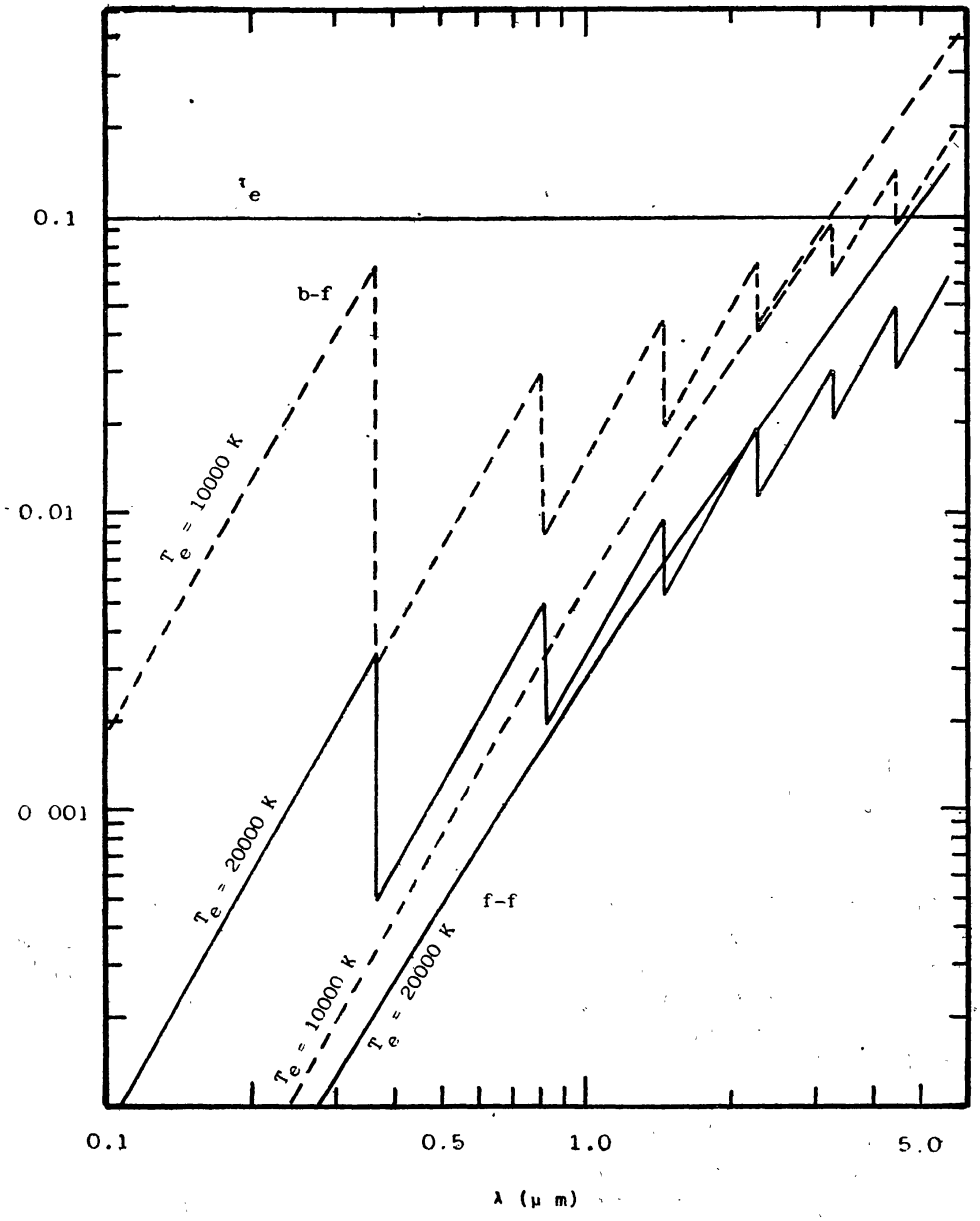

Figure 5. Optical thickness of hydrogen gas in LTE. Electron number density is $N_e = 3 \times 10^{11}$ cm^{-3} and the length $R = 7.2\ R_\odot$, which yields the optical thickness for electron scattering $\tau_e = 0.1$. The optical thicknesses for bound-free and free-free absorption are shown for $T_e = 20{,}000$ K (solid line) and $T_e = 10{,}000$ K (broken line).

front of the stellar disc, the colour will become bluer. This absorption behaviour is generally consistent with observations.

In actual cases of Be envelopes, it is obvious that the non-LTE effects become essential and overall effects of scattering, emission and absorption will yield a wide variety of resultant energy distribution and the wavelength dependence of polarization in some complicated way. Further study well coordinated from a wide spectral region in polarimetry and photometry is highly desirable.

4. Emission lines

4.1. Emission mechanisms

The emission lines in lower members of the Balmer series of Be stars are, as seen in section 2.3, generally formed through the incomplete Rosseland cycle in their cool envelopes. Be stars often reveal emission components in lines other than Balmer lines; Fe II and He I lines are also explained by similar a Rosseland cycle (Wellman 1952a, b, c, 1955).

In contrast, the emission line of O I λ8446 has been attributed to the Bowen fluorescence mechanism in hydrogen Lyman β radiation, since the correlation between emission intensities of O I λ8446 and of lower Balmer lines is well established (see Briot 1981b and references therein). Bruhweiler *et al.* (1982) have also proposed the Bowen mechanism for the Mg II doublet at λ2800, which often appears in emission in early Be stars.

For the Ca II infrared triplet λλ8498, 8542 and 8662 Å, the emission mechanism is not yet clear. Polidan & Peters (1976) and Polidan (1976) found no correlation between emission intensities of this triplet and any parameters of Be stars, and they suggested the possibility of binary interaction as the reason. Briot (1981b) found that the Be stars showing emission lines in this triplet exhibit infrared excess slightly higher than the stars without Ca II emission.

4.2. Emission line intensities

Briot (1971) and Briot & Zorec (1981) have derived a well established relation between emission intensities of Balmer lines and the spectral types of Be stars, in the sense that the emission equivalent width of the Hα line declines while the Balmer decrement increases, on average, along the spectral sequence. Their results are summarized in table 2.

Table 2. Observed Balmer emission intensity (Briot 1971)

Spectral type	B0 – B1	B2	B3	B5 – B6	B7 – B8
Emission equivalent width of *Hα*					
Wα (A)	32(7)	30(12)	24(16)	20(11)	13(9)
Balmer decrements					
Hα/Hβ	2.1 (7)	3.3 (12)	3.9 (16)	5.2 (11)	8.1(9)
Hγ Hβ	0.66(6)	0.56(10)	0.53(7)	0.33(5)	—
Hδ/Hβ	0.60(4)	0.27(4)	0.36(5)	—	—
Hε/Hβ	0.55(2)	0.09(1)	0.22(2)	—	—

Note : The figure in the parenthesis denotes the number of stars for which the values are averaged.

Theoretical predictions of the Balmer decrement Hα/Hβ based on the static and moving-envelope approaches are shown in figure 6, together with the observed average values in table 2. Relative level population N_3/N_4 in the LTE state is also illustrated for comparison.

As an example of static approach, figure 6 gives the theoretical curves of Kogure's (1959b) case V, in which a constant optical thickness for the Lyman continuum is assumed. One may see that observed values distribute along a constant value of the dilution factor W, *i.e.*, the average dimension of envelopes relative to the stellar radii do not vary appreciably along the spectral sequence. The emergent flux of Hα calculated in this case can also explain the spectral dependence of $W\alpha$ in table 2.

Moving-envelope approach of Sobolev (1947) can also qualitatively reproduce the spectral dependence of $W\alpha$ and Hα/Hβ. Some of the theoretical decrements,

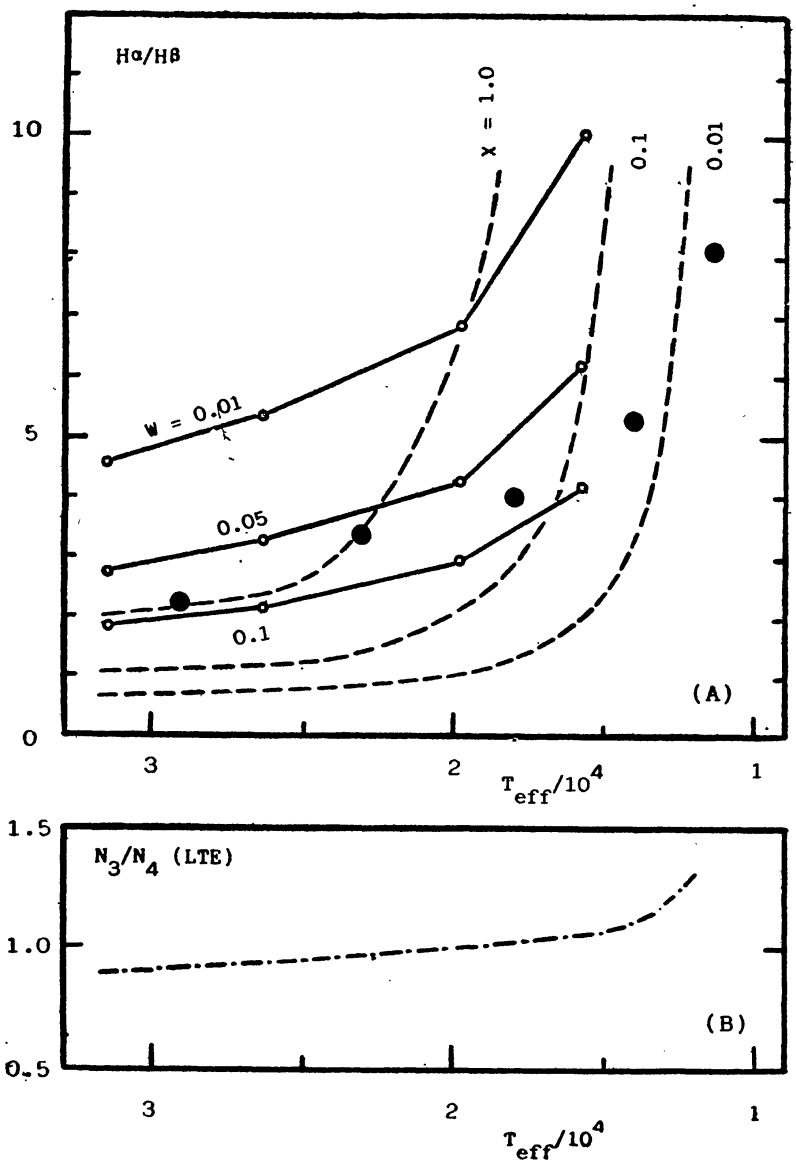

Figure 6. (A) Balmer decrements Hα/Hβ along the spectral sequence calculated by the static (Kogure's case V) and moving-envelope (Lacoarret 1965) approaches. Filled circles show the average observed decrements taken from table 2. (B) Relative level population N_3/N_4 in the LTE state is illustrated for comparison.

calculated by Lacoarret (1965) by this approach, are shown in figure 6, where the parameter x denotes β_{12}/W, β_{12} being the escape probability of the Lα photons. Then, if the velocity gradient does not vary among Be stars, the curves in figure 6 again correspond to the case of constant optical thickness for the Lyman continuum as in case of Kogure (1959b).

The Balmer decrement Hn/Hβ is roughly expressed in Sobolev's method by

$$\frac{\mathrm{H}n}{\mathrm{H}\beta} = \frac{16}{n^2}\left(\frac{\nu_{2n}}{\nu_{24}}\right)^4 \frac{\langle N_n/N_2\rangle}{\langle N_4/N_2\rangle} \approx \frac{16}{n^2}\left(\frac{\nu_{2n}}{\nu_{24}}\right)^4 \frac{\langle N_n\rangle}{\langle N_4\rangle}. \tag{4-1}$$

This expression is also applicable to the static approach, since Hn/Hβ is essentially given by the ratio of source functions for the corresponding lines. In this sense we can transform the Balmer decrement into the respective population ratio and can compare with LTE-values which are also given in figure 6 under the assumption of $T_e = 0.75\ T_{eff}$ (Gehrz *et al.* 1974). It is seen that the LTE population ratio increases toward later spectral type by a factor of about 1.6 from 0.8 at T_{eff} = 29000 K to 1.27 at T_{eff} = 12500 K. Since the non-LTE effects give rise to over-population in the lower level, the spectral dependence of Balmer decrements in theory and observations suggests that the non-LTE effects tend to increase toward late type Be stars.

Another implication from figure 6 is the question: Why nearly constant optical thickness for the Lyman continuum is realized along the spectral type of Be stars ? Such constant optical thickness requires the condition that the electron density of envelopes in early type Be stars should be one order of magnitude higher than in late type Be stars, if the envelope dimensions are not so different from each other, *i.e.*, the dilution factor W is nearly constant.

We next consider the Paschen decrement Pn/P14 ($11 \leqslant n \leqslant 24$) and Paschen-Balmer relative intensities P14/Hβ, based on Briot's (1981a) data, according to which the values of P14/Hβ are generally much higher than those predicted by the Sobolev theory, except for B0e — B1e stars. The Paschen decrements appear rather insensitive to the spectral sequence in her data.

In the frame of Sobolev expression, we can write the Paschen decrements as

$$\frac{\mathrm{P}n}{\mathrm{P14}} = \frac{N_n A_{n,3}\beta_{3,n} h\nu_{3,n}}{N_{14}A_{14,3}\beta_{3,14}h\nu_{3,14}} \approx \begin{cases} \dfrac{b_n}{b_{14}}\left(\dfrac{N_n}{N_{14}}\right)^* \dfrac{A_{n,3}\nu_{3,n}}{A_{14,3}\nu_{3,14}}, \\ \qquad \text{(for optically thin case)} \\ \dfrac{b_n}{b_{14}}\left(\dfrac{14}{n}\right)^2 \left(\dfrac{N_n}{N_{14}}\right)^* \left(\dfrac{\nu_{3,n}}{\nu_{3,14}}\right)^4, \\ \qquad \text{(for optically thick case)} \end{cases} \tag{4-2}$$

where $(N_n/N_{14})^*$ denotes the LTE value. Here we notice that the deviation factors b_n nearly take the LTE value ($b_n \sim 1$) for $n \gtrsim 10$, according to the model calculations by Kříž (1979b) or Poeckert & Marlborough (1978b). In figure 7 are shown the Paschen decrements Pn/P14 for both cases of optically thin and thick, together with the observed values by Briot (1981a). Good agreement with observations is remarkable in the optically thin case. This result implies that the Be envelopes are optically thin for the Paschen lines higher than $n \cong 15$.

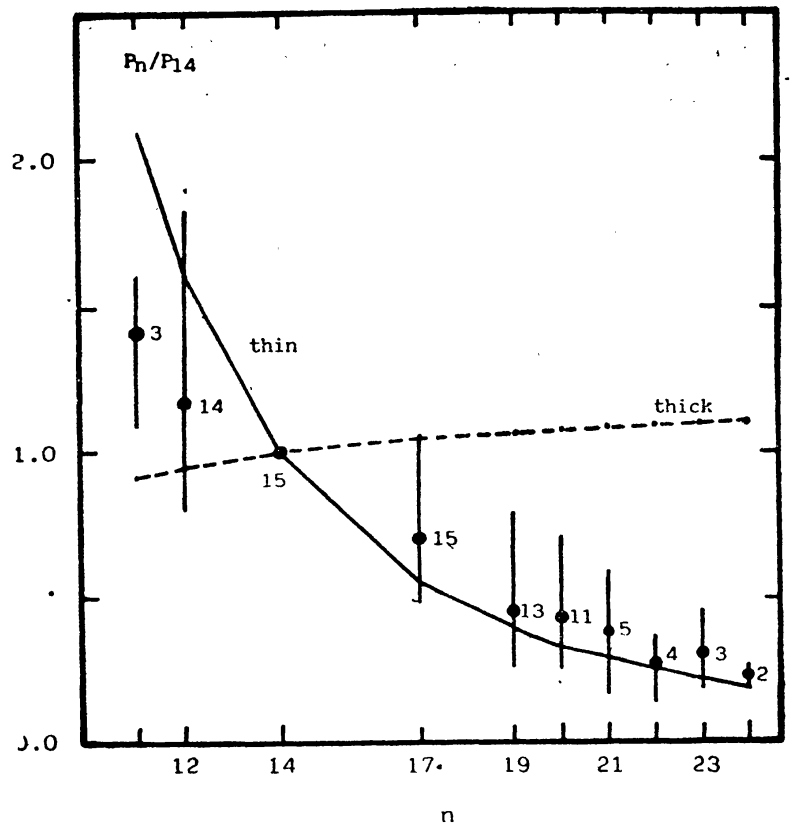

Figure 7. Paschen decrements P*n*/P14 ($n = 11 \sim 24$). The mean observed decrements are shown by filled circles with the scatter around the mean, and the numbers of stars used for taking the average are also shown. Theoretical predictions are illustrated in the cases of optically thin (solid line) and optical thick (broken line) for both of which $b_n = 1$ is assumed. One may notice that the optically thin case well coincides with observations.

Then, if we adopt the optically thin case, the Paschen-Balmer relative intensities P*n*/Hβ can be written as

$$\frac{\mathrm{P}n}{\mathrm{H}\beta} \propto \frac{b_2}{b_4}\left(\frac{N_n}{N_4}\right)^* N_2^*, \tag{4-3}$$

where the level populations with asterisk denote the LTE values. In the frame of this expression, strong Paschen lines should be attributed to strong enhancement in the b_2-factor relative to b_4-factor, possibly due to the opaque nature of Be envelopes in the Lyman and Balmer continua. In fact, Be stars having Paschen emission lines are characterized by strong Hα emission (Briot 1981a).

Finally we present the ($W\alpha$ — Hα/Hβ) diagram, which was calculated by Kogure, Hirata and Suzuki (1975, personal communication) using the method of Kogure (1969b). An example of their calculation is illustrated in figure 8. In the calculation the envelope is assumed to be a disc or ring of constant vertical thickness $2R_*$ and with equatorial extension from R_1 (inner radius) to R_2 (outer radius).

The parameters adopted in the calculations of theoretical curves in figure 8 are as follows: $T_{UV} = 30{,}000$ K (stellar temperature in the Lyman continuum region), $T_{eff} = 24{,}000$ K (effective stellar temperature in the optical region), $T_e = 24{,}000$ K (electron temperature in the envelope), $V_* = 400$ kms^{-1} (stellar equatorial rotational

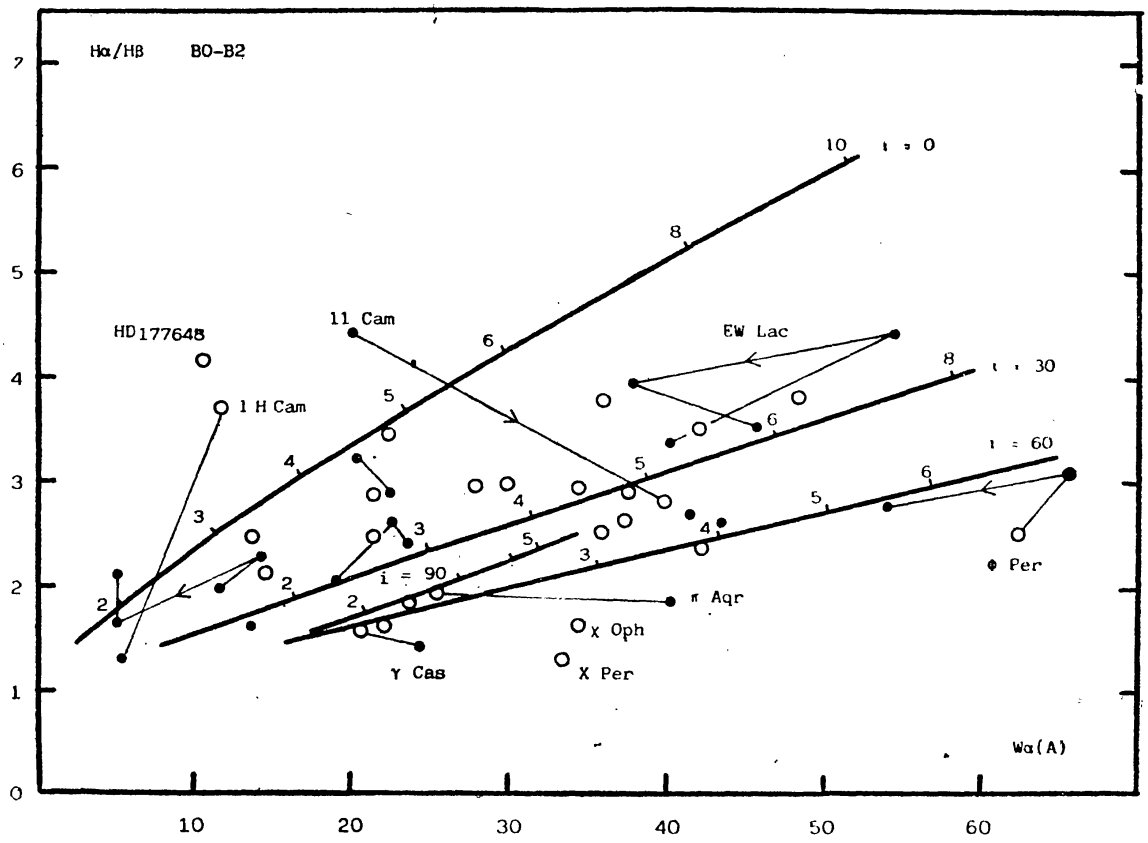

Figure 8. Correlation between Balmer decrement Hα/Hβ and Hα emission equivalent width W_α for early type Be stars. The observed values are taken from Briot (1971) (open circles) and from our observations at the Okayama Astrophysical Observatory (filled circles). The same stars observed by different observers or observed at different epochs are connected by thin lines. The theoretical curves (thick lines) are those calculated by Kogure *et al.* (1975). The adopted parameters are given in the text. The outer radii R_2/R_* marked in each of theoretical curves show the values in case of $j = 1$ (case of angular momentum conservation).

velocity), $\tau_{Bc} = 1.0$ (optical depth of the whole envelope in the Balmer continuum). $H = 2R_*$ (total height), $R_1 = R_*$ (disc case) and $i = 0°, 30°, 60°, 90°$ (inclination angle of the rotational axis). The calculated values of $W\alpha$ and the decrement Hα/Hβ are given as a function of R_2/R_* for each case of inclination angle i. The values of R_2/R_* are marked on the calculated curves in figure 8. If the envelope has a ring-like structure, *i.e.*, $R_1/R_* > 1$, then the theoretical curves will shift upwards giving a steeper Balmer decrement with smaller emission equivalent width $W\alpha$.

In figure 8, observed values for B0Ve — B2Ve, are taken from Briot (1971) and from our observations at the Okayama Astrophysical Observatory. The same stars observed by different observers or observed at different epochs are connected by thin lines. Although a large scatter is seen in the distribution of stars, most of the scatter can be explained by the variety of parameters i, H, R_1, R_2 and τ_{Bc}. The significance of figure 8 as a tool of diagnostics of Be envelopes will be given later (sections 6.2, 6.3).

4.3. Emission line profiles

The emission lines of Be stars are typically characterized by symmetric double-peaked profiles, including, as special cases, single peaks (pole-on stars) and double-peaks with central shell absorption (shell stars).

We first consider the profile formation in an illustrative case of axially symmetric, purely rotating thin envelope. This envelope is extending from $r_1 = R_1/R_*$ (inner radius) to $r_2 = R_2/R_*$ (outer radius) in the equatorial plane and is seen from an inclination angle $i (i \neq 90°)$. Let $B(r)$ and $\psi(v)$ be the surface brightness and the intrinsic line-broadening function, respectively, where $r = R/R_*$ and v denote the relative radius and the radial velocity inside a profile, respectively. Then the emission line profile $E(v)$ can be written as

$$E(v) = \int_{r_1}^{r_2} \int_{-\pi}^{+\pi} d\phi \, dr.r \, B(r) \, \psi(v - v_l(r, \phi)), \tag{4-4}$$

where $v_l(r, \phi)$ denotes the line-of-sight velocity at the point (r, ϕ). We also assume that the function $\psi(v)$ is independent of the position in the envelope, and that the occultation of the envelope by the star is negligible.

For simplicity we approximate the circular velocity $v_\phi(r)$ and the surface brightness $B(r)$ by the following power law functions

$$v_\phi(r) = v_\phi(1) \, r^{-j}, \; B(r) = B_1 r^{-m}, \tag{4-5}$$

where j and m are constant, The values of $j = 1$ and $1/2$ correspond to the cases of angular momentum conservation and the Keplerian motion, respectively. When $j = 1/2$, $v_\phi(1)$ should be the break-up velocity, $\sqrt{GM_*/R_*}$, and, when the circular velocity is smoothly linked to the stellar rotation, we have $v_\phi(1) = V_*$.

Introducing new variables and orthogonal systems as

$$Z = r^j, \quad u = v/[v_\phi(1) \sin i],$$

$$\eta = \frac{\sin \phi}{Z}, \quad \xi = \frac{\cos \phi}{Z},$$

we can transform equation (4-4) into the form

$$E(u) = \frac{2B_1}{j} \int_{-1/Z_1}^{+1/Z_1} \Lambda(\eta) \, \psi(u - \eta) \, d\eta, \tag{4-6}$$

where

$$\Lambda(\eta) = \int_{\xi_2(\eta)}^{(1/Z_1^2 - \eta^2)^{1/2}} (\xi^2 + \eta^2)^{-p} \, d\xi, \tag{4-7}$$

$$p = \frac{2 - m}{2j} + 1, \; Z_n = r_n^j \; (n = 1, 2) \tag{4-8}$$

and

$$\xi_2(\eta) = \begin{cases} 0, & \text{for } \dfrac{1}{Z_2} \leqslant |\eta| \leqslant \dfrac{1}{Z_1} \\ \sqrt{1/Z_2^2 - \eta^2}, & \text{for } |\eta| < 1/Z_2 \end{cases} \tag{4-9}$$

The first implication of equation (4-6) is that the resultant profile $E(u)$ is completely determined by the parameters p, Z_1 and Z_2, except for the proportional constant. That is, the same profile is obtainable by different combination of j and m, if the values of p, Z_1 and Z_2 are kept unchanged. This property has been first proved in more general case by Huang (1972). It is probably by this property that the observed profiles could be fitted with theoretical ones which are deduced under different value of j. Actually, Hutchings (1970, 1971) and Kogure (1969a) assumed $j = 1$, whereas Marlborough & Cowley (1974), Marlborough (1976) and Kříž (1976b, 1979b) adopted $j = 1/2$.

We consider the emission line profiles and peak separation v_P on the basis of equation (4-6). The latter is defined as the half separation of blue and red peaks in velocity unit. Furthermore, let us assume that the intrinsic broadening is negligibly small, *i.e.*, we have $\psi(u - \eta) = \delta(u - \eta)$, δ being the Dirac function. Then equation (4-6) can be reduced to

$$E(u) = \frac{2B_1}{j}\Lambda(u). \tag{4-10}$$

Figure 9 illustrates the profiles $\Lambda(u)$ for non-detached ($Z_1 = 1$) and infinitely extended ($Z_2 \to \infty$) envelopes with $p = 0$, 1, 2 and 3. In cases of $p = 1$ and 2 the profiles for $Z_2 = 2$ and 3 are also shown. One may see that, when p (> 0) is fixed, the emission intensity is getting stronger and the peak separation smaller as the outer radius Z_2 increases. It is also evident that the peak separation is given by

$$u_P = 1/Z_2,$$

or

$$v_P = v_\phi(1) \sin i/r_2^j \equiv v_\phi(r_2) \sin i. \tag{4-11}$$

If the intrinsic broadening function $\psi(v)$ has a half-width exceeding the peak separation v_P, the resultant profile turns into a single-peaked one.

Equation (4-11) indicates that the peak separation v_P is a good measure of the outer radius r_2 in the sense that, if we know the circular-velocity law, *i.e.* the value of j, we can estimate the value of r_2 from the measurements of v_P and $v_\phi(1) \sin i$. The latter is ordinarily regarded as $V_* \sin i$, though the break-up velocity must be used in principle in the case of Keplerian motion, *i.e.* $j = 1/2$. This general relation also holds in cases of equator-on view ($i = 90°$) (Sobolev 1947, 1960), and of elliptical rings (Huang 1972, 1973).

The emission line profiles are characterized by some widths such as the half total-width, v_T, the half half-width, v_E, and the peak separation, v_P. If the broadening of emission lines is purely rotational and $v_\phi(1) = V_*$, we should have $v_T \leqslant V_* \sin i$, reflecting the structure (disc or ring) of envelopes, since the wing parts of profiles are usually formed in the inner regions of envelopes. The measurements of v_T for lower Balmer lines which have been made by Doazan (1970), Slettebak (1976) and Andrillat & Fehrenbach (1982) reveal a large scattering against the values of $V_* \sin i$. Thus, a considerable fraction of Be stars exhibit extended wings ($v_T \gg V_* \sin i$), particularly in Hα and Hβ, suggesting the existence of some

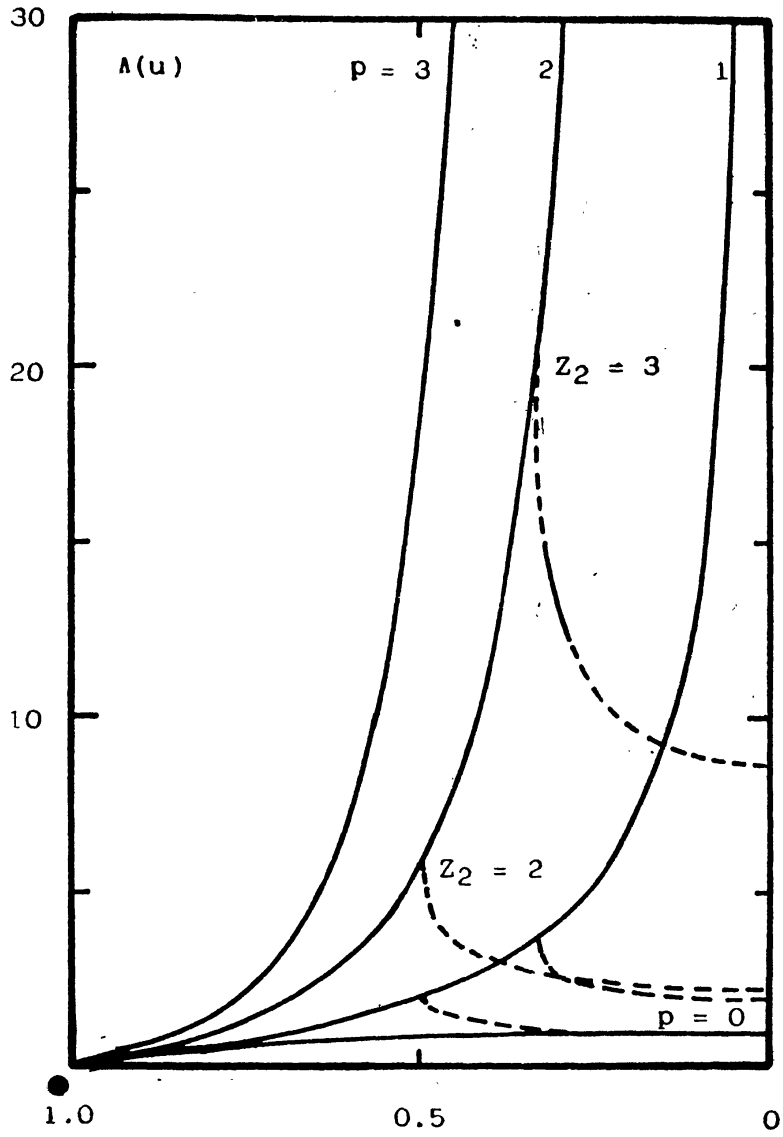

Figure 9. The emission line profile $\Delta(u)$, calculated for axisymmetric, rotating, thin and non-detached disc in case of $p = 0, 1, 2$ and 3. The solid line corresponds to the infinite outer radius, and the broken lines illustrate the profiles in case of finite envelope for $Z_2(= r_2^j) = 2.0$ and 3.0 for each of $p = 1$ and 2.

other broadening agency such as electron scattering (Marlborough 1969; Poeckert & Marlborough 1979). At the same time, there are also stars showing narrow lines ($v_T < V_* \sin i$). A natural explanation is that they have detached envelopes, *i.e.* rings.

The difference $v_T - v_P$ may be a measure of the equatorial extension, $r_2 - r_1$, since v_P gives the information about r_2. In many cases, values of $r_2 - r_1$ thus estimated are not small as compared with the stellar radius R_* even in case of ring-like structure. This conclusion is consistent with that of Kříž (1979b).

The distribution of stars on the ($v_P - V_* \sin i$) diagram also exhibits large scattering in the region beneath the line of $v_P = V_* \sin i$. According to equation (4-11), this scatter is attributable to that of r_2^j, *i.e.* to the difference in the outer

radii of envelopes. It is also to be mentioned that the observed peak separation in various lines discloses a kind of stratification, since the values of v_P generally increase in the order of Hα, Hβ, ..., He I and Mg II λ4481 (Hutchings 1970, 1971). The values of v_P in He I and Mg II λ4481 are often close to V_* sin i, thus indicating a stratified and wide extension of Be envelopes on the equatorial planes.

Finally we remark on the peak separation of shell stars, because strong shell absorption component might broaden the peak separation of emission components. In this context, we can notice that, even in shell stars, the peak separation is smaller in the lower Balmer lines where the opacity is larger. As another example, we can see the variation of peak separations of Balmer emission lines observed in Pleione in the recent shell phase, that is, the peak separation has decreased as the development of shell characteristics (Hirata & Kogure 1977). In this way we can conclude that the arguments on peak separation of ordinary Be stars also hold in shell stars as they are.

5. Shell absorption lines

5.1. General appearance

It is generally accepted that the shell absorption lines of Be stars are formed in the part of cool envelopes extending in front of the stellar discs. Depending on the structure of cool envelopes, shell lines appear in the Balmer lines as well as in metallic lines in a wide variety of forms.

For the Balmer shell lines the values of n_l, the last principal quantum number of visible shell lines, may be a measure of the development of shell line spectra. Thus the stars are sometimes called weak shell stars when n_l is small as in, say, ψ Per ($n_l = 10 \sim 12$), and are called strong (or developed) shell stars when n_l is large as in EW Lac ($n_l = 35 \sim 40$). It is also to be noticed that many Be stars sometimes show the shell absorption cores in lower Balmer members (Hubert-Delplace & Hubert 1979; Jaschek *et al.* 1980; Slettebak 1982).

The shell lines other than hydrogen are visible in many species covering a wide range of excitation stage. Their appearance in line widths, profiles, and radial velocities is generally similar to the hydrogen shell lines. In table 3 the number of shell lines identified in the spectral range λλ3550–4855 Å are given for EW Lac (B3: IV: e-shell, V_* sin i = 300 km s^{-1}, Slettebak 1982) at the epoch 1965/7 (Kupo 1969) and 1978/9 (Poeckert 1980), and for Pleione (B8 (V:) e-shell, V_* sin i = 320 km s^{-1}, Slettebak 1982) in 1977 (Ballereau 1980). The atoms and ions are separately given according to their ionization stage and ionization potentials (I. P. $\gtrsim$ 10 eV in neutral atoms, and I.P. (I → II) $\gtrsim$ 10 eV in singly ionized ions). The linear dispersion of spectrograms used is 15 and 30 Å mm^{-1} in Kupo (1969), 6.7–9.7 Å mm^{-1} in Poeckert (1980), and 12 Å mm^{-1} in Ballereau (1980). One should notice that almost all metallic lines arise from the metastable levels.

In table 3 one may see the general appearance of metallic shell lines, along with their marked time variation in case of EW Lac. It is seen that the shell spectrum of EW Lac in 1965/7 was fully developed, showing high stage of ionization, while the ionization stage decreased in 1978/9 almost to that of Pleione. In any case the ionization and excitation state is lower than that of photospheric spectrum in a

Table 3. Number of shell absorption lines detected in the spectral range λ3550–λ4855 Å, except Hydrogen

1. Neutral atom

Z	Atom	EW Lac 1965/7 Kupo (1969)	EW Lac 1978/9 Poeckert (1980)	Pleione 1977 Ballereau (1980)
I.P. < 10 eV				
11	Na I	0	0	1
12	Ng I	3	3	4
13	Al I	2	1	1
20	Ca I	9	0	6
21	Sc I	0	1	0
22	Ti I	0	5	0
23	V I	0	6	0
24	Cr I	1	9	2
25	Mn I	0	1	0
26	Fe I	157	47	105
27	Co I	0	3	0
28	Ni I	4	5	0
38	Sr I	0	1	0
40	Zr I	1	1	0
I. P. > 10 eV				
2	He I	5	0	0
8	O I	0	0	1
10	Ne I	1	0	0
18	Ar I	5	0	0

2. Singly ionized ions

Z	Ion	EWLac 1965/7	EWLac 1978/9	Pleione 1977
I. P. (I → II) < 13 eV				
5	B II	1	0	0
12	Mg II	3	1	3
13	Al II	4	0	0
14	Si II	4	5	7
19	K II	1	0	0
20	Ca II	1	2	3
21	Sc II	0	5	16
22	Ti II	24	52	66
23	V II	29	19	33
24	Cr II	24	42	41
25	Mn II	0	6	2
26	Fe II	26	74	85
27	Co II	0	0	1
28	Ni II	0	4	9
38	Sr II	0	2	2
39	Y II	0	0	16
40	Zr II	1	0	9
42	Mo II	0	0	5
I. P. (I → II) < 10 eV				
6	C II	1	0	0
7	N II	5	0	0
8	O II	30	1	0
9	F II	1	0	0
10	Ne II	5	0	0
15	P II	1	0	0
16	S II	19	0	0
17	Cl II	11	0	0
18	Ar II	13	0	0

3. Doubly ionized ions

16	S III	2	0	0
20	Ca III	1	0	0
26	Fe III	5	0	0

majority of shell stars, except some ones which exhibit ionization state comparable to that of the photosphere, *e.g.* 27 CMa (B3III(e) p-shell, $V_* \sin i = 150$: km s^{-1}, Slettebak 1982) and HD 184279 (B0.5, Jaschek *et al.* 1980, $V_* \sin i = 200$ km s^{-1} in new Slettebak system). In this sense the envelopes are *cool*, though the excitation temperature can vary in some range as seen in EW Lac. A wide range of ionization state in a star also suggest the stratification existing inside the envelope.

5.2. Curves of growth

The curve of growth provides one of the basic tools in the spectrophotometric studies of normal stellar spectra. Though the envelopes of Be and shell stars are different in their non-LTE nature from the normal stellar atmospheres, the method of curve-of-growth has been applied to the analysis of shell absorption lines since the first work of Underhill (1949). Since then, Underhill (1952, 1954), Özemre (1967), and others have applied this method mainly aiming to deduce the excitation temperature T_{ex} and turbulent velocity v_t inside the envelopes. The derived values of T_{ex} mostly fall in a range of 8000–10000 K, reflecting the *cool* nature of envelopes. In contrast, the values of v_t exhibit rather large scatter from several to several tens km s^{-1} for different ions (Özemre 1967), or for different epochs of observations (Underhill 1954).

In figure 10 is illustrated an example of curve of growth constructed by Higurashi & Hirata (1978) for Pleione, and table 4 gives a part of their derived parameters. The excitation temperature thus found scatters in a range of 8000–13000 K

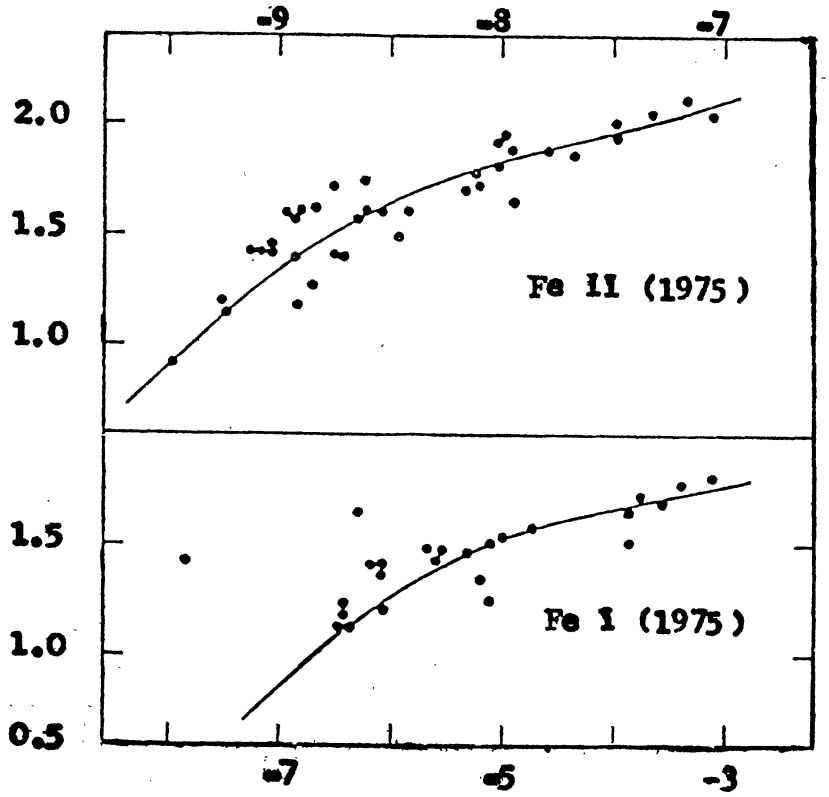

Figure 10. Curve of growth of the Fe II and Fe I lines of Pleione in 1975 (Reproduced from Higurashi & Hirata 1978).

Table 4. Physical parameters of Pleione derived from the curve-of-growth analysis (Higurashi & Hirata 1978)

Epoch	Ion	n	T_{ex}(K)	$\log\langle Nl\rangle$	v_t(km s^{-1})
1975	Fe I	24	8400	15.4	3.8
	Ti II	31	10500	15.9	4.5
	Fe II	28	10080	18.0	5.7
	Cr II	21	13260	15.9	5.7
1976	Fe I	31	7520	15.7	3.9
	Ti II	33	9880	16.1	4.7
	V II	8	10950	15.7	3.8
	Fe II	38	9000	18.3	6.0
	Cr II	21	12000	16.1	6.0

Note : n, total number of lines used; T_{ex}, excitation temperature; $\langle Nl\rangle$, column density in cm^{-2}; v_t, microscopic velocity.

with the weighted mean of 9900 $\pm$ 400 K for 1975 and 9100 $\pm$ 400 K for 1976. It is also noticed that the excitation temperature is definitely lower in neutral iron than in singly-ionized metals. Similar tendency can be seen in turbulent velocities. In addition they derived the column densities of ions log $\langle Nl\rangle$ in cm^{-2}, from which they estimated the mass of envelope in the order of 10^{-10} $M_\odot$.

In this way the curves of growth enable us to deduce several physical parameters expressing some average state of envelopes. However, one should recall the basic assumptions of the curve-of-growth technique, which has been developed in case of normal stellar atmospheres. When we apply this technique to the shell lines, it is inevitable to assume the same degree of metastability, that is, the same values of deviation factor b_n for all metastable states and for ground state. Usually one assumes $b_n \fallingdotseq 1/W$ by an implication from the modified Saha equation. If this assumption be valid, the linear part of a curve of growth yields the values of mean column density averaged over the stellar surface and of mean excitation temperature in ion formation region concerned.

However, the turbulent velocity v_t thus derived does not give the true turbulent velocity, since the existing velocity gradient makes the lines desaturate and hence makes the apparent turbulent velocity larger (Abhyankar 1964; Arakelyan 1969; Mihalas 1979). Continuous emission of the envelope also obscures the true equivalent widths, contributing to the vertical shift of the curves of growth in question (Underhill 1949). If a stellar disc of its fractional area β is occulted by the envelope, as seen in the next section, then the observed equivalent widths will be reduced by the same fraction β. All these factors mentioned above will affect the apparent turbulent velocity, and make the interpretation of v_t difficult.

5.3 Central depths

Let β be the fractional area of the stellar disc occulted by the envelope and τ_α be the mean optical depth of the envelope at the line centre of the Hα line. If there appears no appreciable Balmer progression, the central depths of the Balmer shell lines as the function of the series number n provide a technique to deduce the values of β and τ_α (Kogure 1969b). If we define the central depth $R_n = 1 - r_n/r_n^*$ where r_n^* and r_n denote the residual intensities of the photospheric and shell absorption

lines, respectively, relative to the adjacent continuum, then the value of R_n for the Hn line can be expressed (Kogure *et al.* 1978), as

$$R_n = \beta\{1 - \exp[-\omega_n \tau_\alpha]\}, \quad (5\text{-}1)$$

where $\omega_n = (B_{2n}\nu_{2n})/(B_{23}\nu_{23})$, B_{2n}, B_{23} being the Einstein coefficients and ν_{2n}, ν_{23}, the frequencies of respective $2n$-, 23-radiations. Plotting observed central depths on the (R_n — log ω_n) diagram, and adjusting the theoretical curves (5-1) so as to fit with observations, we can get the values of β and τ_α.

This method has been applied to EW Lac by Kogure (1975) and to Pleione by Hirata & Kogure (1977, 1978). Hirata & Kogure (1977) have extended it to the case where the envelope can be approximated by two sublayers with different optical depths $\tau_{\alpha i}$ and fractional areas $\beta_i (i = 1, 2)$. Figure 11 illustrates an example of the fitting in case of Pleione. An extension to the metallic shell lines has been made by Higurashi & Hirata (1978).

5.4. *Balmer progression*

When the radial velocity v_n at the centre of shell line Hn varies along the series number n, *i.e.*, when a gradient $dv_n/dn \gtrless 0$ exists, we call this phenomenon the Balmer progression. There are at present two opposite points of view to interpret the Balmer progression. One is to attribute it to an effect of Balmer reemission, while the other is to attribute it to an absorption process.

The former explanation was used by Marlborough & Gredley (1972) who calculated the line profiles based on Marlborough's (1969) method. Their theoretical prediction, however, was unsuccessful to reproduce the observed Balmer progression which appeared in Pleione in 1938–1954. Similar effort has been made by

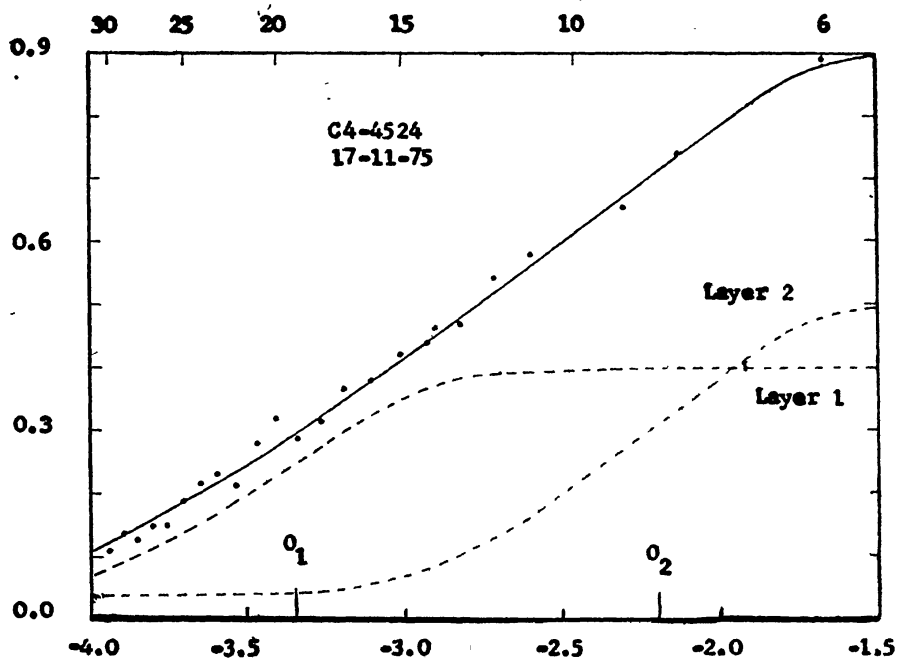

Figure 11. Fitting of central depths of the Balmer shell-absorption lines for Pleione in 1975. The broken lines denote the theoretical curves for two sublayers with different optical depth τ_α and fractional area β. The full line gives the composite theoretical curves to be compared with observed points which are plotted by dots. (Reproduced from Hirata & Kogure 1977).

Peraiah (1982) by showing that the higher members of the Balmer lines are formed in a region where the velocity gradient is steep. In this case, the next step should be taken to see how Balmer progression can be predicted by such differential reemission.

The second explanation, of absorption process, is based on the fact that contrary to the cases of supergiants and P Cyg stars the progression in Be stars occurs also in higher Balmer members, for which no emission component is expected. We present here a simple prediction as an application of the central-depth method given in section 5.3. Let $R_n(v)$ be the depth of Hn-line profile at the radial velocity v, then the value of $R_n(v)$ can be written as

$$R_n(v) = \beta(v)\{1 - \exp[-\omega_n \tau_\alpha(v)]\}, \tag{5-2}$$

where β, τ_α have the same meaning as in equation (5-1), except that they depend on v.

The appearance of Balmer progression can be shown by a simple example. Let us consider two radial velocities $v_i (i = 1, 2$, and $v_1 > v_2)$, and draw the depth $R_n(v_i)$ as a function of n, for the constant values of v_i. Figure 12(a) illustrates schematic

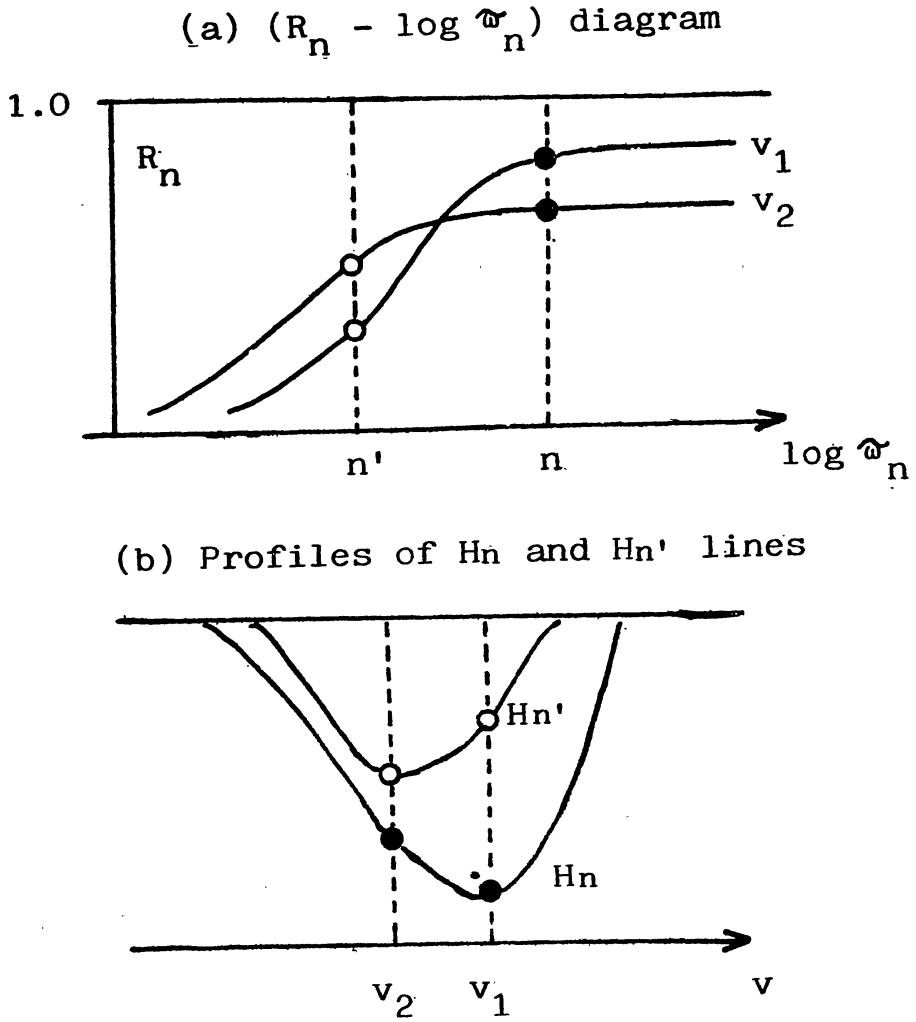

Figure 12. (a) Schematic (R_n — log ω_n) diagram in two particular velocities v_1 and $v_2(v_1 > v_2)$ inside the shell absorption profiles of the Balmer series.
(b) Schematic profiles of shell absorption lines in the Hn and H$n'(n' > n)$, which exhibit the Balmer progression in a type of $dv_n/dn < 0$.

curves of the (R_n — log ω_n) relation for v_1 and v_2, where $\beta(v_1) > \beta(v_2)$ and $\tau_\alpha(v_1) < \tau_\alpha(v_2)$ are assumed. If we consider the profiles of two different lines of Hn and Hn' ($n' > n$), the expected profiles of these lines may be such as schematically shown in figure 12(b).

Figure 12(b) predicts for Balmer progression $dv_n/dn < 0$. The problem is then how to find the velocity field which gives the $R_n(v)$ curves such as shown in figure 12(a). Using this idea, Hirata (1982b) has searched for possible velocity field which gives rise to typical cases of Balmer progression, and found two possible cases of (i) precessing elongated disc and (ii) decelerating outflowing envelope. These considerations are efforts to find the simplest geometry and velocity field to yield observed progression. Another possibility is an introduction of multilayers, by which multiple maxima in $\tau_\alpha(v)$ are realized. In fact, Merrill & Sanford (1944) originally introduced the rapid and slow decrements for the progression in 48 Lib. Although detailed examination is not yet finished, these examples suggest a possible way to explain the Balmer progression in terms of pure absorption process. It is also possible that the emission process may play some role in the occurrence of Balmer progression in the lower Balmer members.

6. Structure of cool envelopes

6.1. Diagnostics of the structure

In the previous sections we have separately considered the spectral formation of the continuum, emission and shell absorption lines. The next step is to construct reliable ad-hoc models for individual stars and for Be stars in general. Although a number of ad-hoc models has so far been proposed, most of them are based on some particular picture of envelopes such as rotating thin discs or vertically expanded shells. Before proceeding to the modelling of envelopes, it is obviously desirable to make a sufficient diagnostic on the global picture of envelopes which often show their indications in their spectral behaviour. In spite of its importance, the coordinated diagnostics has not yet been fully developed.

In this section we consider the following structural properties : (a) Are the envelopes really flattened or vertically expanded ? (b) Are the envelopes disc-like or ring-like ? (c) Are the envelopes circular or elongated ? (d) Do the envelopes exhibit inhomogeneities or multiple structure ? And, (e) what circular-velocity law prevails in envelopes ?

The present purpose of diagnostics is limited to pick up the candidate stars having special behaviour. However, if we combine the results, we can expect to obtain a reliable picture of Be-star envelopes for individual stars or in average, even in the present state of diagnostics.

6.2. Flattened or vertically expanded ?

(i) *Polarization*

Most of Be stars exhibit intrinsic linear polarization often variable and of typically 1% in the optical continuum. In figure 13 is shown the spectral-type dependence of the intrinsic polarization, $P(\%)$. The polarization data are taken from those

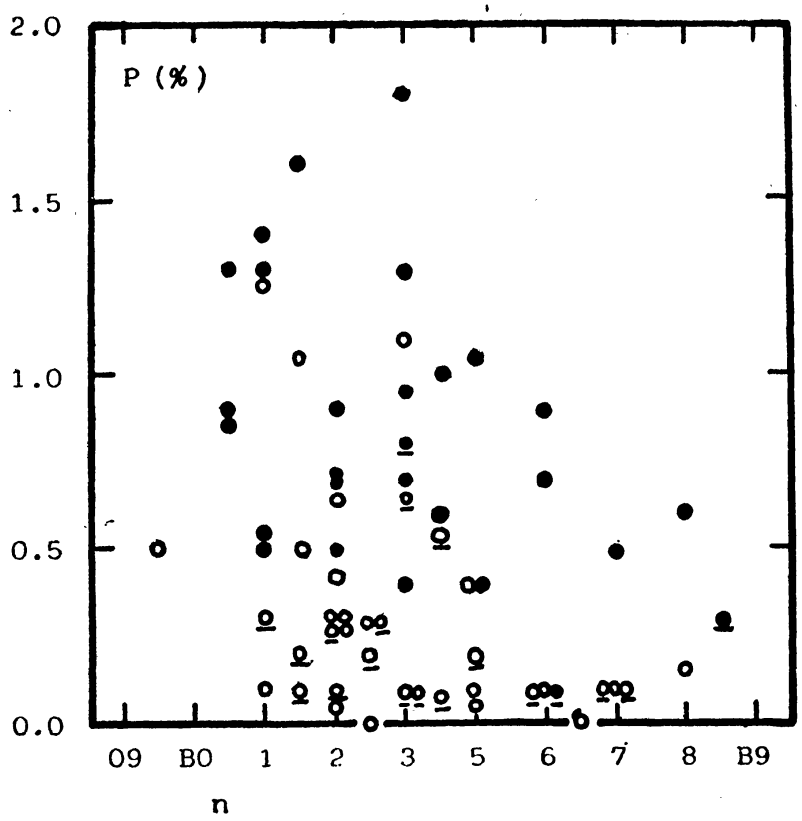

Figure 13. Distribution of the intrinsic linear polarization P (%) along the spectral type. The filled circle indicates the shell stars (defined as Be stars which showed well-developed shell spectra or showed frequently the shell spectra in past). The open circle denotes non-shell stars. The bar under the mark means the upper limit of P.

compiled by McLean & Brown (1978). The effective wavelength of passband is 4250 Å. Spectral types are adopted from Slettebak (1982). One may notice that the upper boundary of $P(\%)$ is appreciably higher in early-type stars than in late-type stars. Metz (1982) has examined the possibility of spherical shell model around the deformed star rotating nearly at its break-up velocity. Even if we admit that the intrinsic polarization is formed in the deformed star (see section 3.2), this model hardly explains the low polarization in late-type Be stars, since late-type stars are generally rapid rotators, nearer their break-up velocities than early-type Be stars (see figure 4 of Paper I).

Since the first work of Coyne & Kruszewski (1969), the intrinsic linear polarization has been attributed to the electron scattering in the flattened envelope (Coyne 1976; Coyne & McLean 1982). Thus, it offers an important tool of diagnostics on the flatness of the envelopes. In case of a point source and an optically thin, purely scattering, axisymmetric envelope, Brown and McLean (1977) derived the expression,

$$P = 2\bar{\tau}(1 - 3\gamma) \sin^2 i, \tag{6-1}$$

where $\bar{\tau}$ is the mean Thomson-scattering optical thickness averaged over solid angle and γ is a shape factor measuring the flatness of the envelope. The value of $\bar{\tau}$ depends on the density, size of envelope and shape of the envelope, while the shape factor becomes zero for a thin equatorial disc and one third for a spherically

symmetric envelope. Expression (6-1) tells us that the shape factor γ cannot be separated from $\bar{\tau}$ in general. Jones (1979) has developed a more elaborate model (finite size of star and inclusion of single scattering of thermal emission created in the envelope) to interpret the wavelength dependence of polarization in the optical and infrared regions. Total vertical height of the disc, H, thus derived, is as small as $0.45 \sim 0.85\ R_*$ and the flatness $H/(R_2 - R_1)$ ranges in $0.08 \sim 0.4$ in his seven well-developed Be stars (R_1 and R_2 are the inner and outer radii of the envelope).

Though the contribution of emission and absorption processes may play an important role in the formation of polarization, as suggested in section 2.3, and by Jones (1979), we here discuss the general trend, based on the expression (6-1) as a rough guess. The dependence of the polarization on the inclination angle has been demonstrated by Poeckert & Marlborough (1976), McLean & Brown (1978) and McLean (1979). McLean & Brown (1978) obtained an inclination-angle free parameter $k = P/(V_* \sin i)^2 = 2\bar{\tau}(1 - 3\gamma)/V_*^2$ less than 3×10^{-7} $(\mathrm{km/s})^{-2}$ with a large scatter in large $V_* \sin i$. This scatter should be attributed to the scatters in $\bar{\tau}$, γ and V_*.

The distribution of polarization along the spectral type (figure 13) closely resembles the distribution of the Balmer line intensity (Briot 1971; table 2 in this article). Balmer line intensity is expected to be an increasing function of $\bar{\tau}$. Thus, one may expect the correlation between the polarization and the Balmer line intensity. In fact, we can see such correlated variation in π Aqr (Nordh & Olofsson 1977; McLean 1979) and in γ Cas (Poeckert & Marlborough 1977; McLean 1979). In figure 14 we

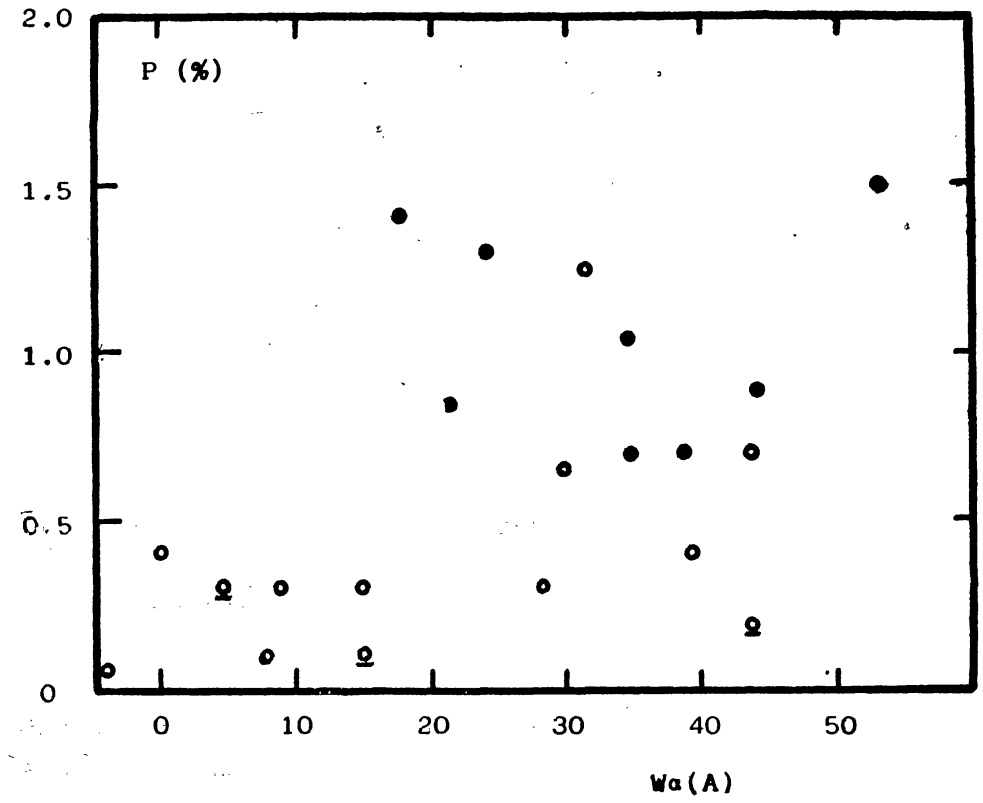

Figure 14. The correlation between the intrinsic polarization and the Hα emission equivalent width in B0–B2 stars. The symbols are the same as in figure 13.

illustrate the correlation between the polarization degree of McLean & Brown (1978) and the mean Hα emission equivalent width obtained by Dachs *et al.* (1981) and Andrillat & Fehrenbach (1982) for early type Be stars (B0–B2). It is seen that the intrinsic polarization of stars with $W\alpha \lesssim 15$ Å is less than 0.5%, and high polarization appears in stars with $W_\alpha \gtrsim 20$ Å. No correlation is found in stars with $W_\alpha \gtrsim 20$ Å. Similar diagrams were constructed by Poeckert & Marlborough (1976) and McLean (1979) and show the same tendency. We have also examined the correlation between the inclination-angle free parameter k and W_α, but no correlation is found. These results imply that relatively large τ is necessary for achieving high polarization and the value of γ may differ in different Be stars. The latter possibility is examined in spectroscopic data in the following subsections.

(*ii*) *Central depths of shell absorption lines*

For the shell stars with sufficiently large values of V_* sin i, the central-depth method given in section 5.3 yields an effective way to pick up stars with vertically thin envelopes. That is, if the derived value of β is less than unity, the vertical height of the envelope should effectively be less than stellar diameter, since such a star can be regarded as equator-on and a part of naked stellar disc can be seen through the unocculted fractional area $(1 - \beta)$.

As a typical example we show the development of shell spectrum of Pleione since the commencement of its recent shell phase in 1972. According to Hirata & Kogure (1977, 1978), the envelope of Pleione is composed of an optically thicker but vertically thinner layer (layer 1) and an optically thinner but vertically thicker layer (layer 2). Layer 1 may be regarded as the densent part of gas distribution in the whole envelope. The time developments of $\tau_{\alpha i}$ and β_i for layer $i (i = 1, 2)$ are illustrated in figure 15, in which one may see that the recent shell phase of Pleione has started from the formation of vertically very thin but optically thick envelope, and then gradually expanded vertically as well as horizontally.

(*iii*) *The appearance of shell absorption lines*

The condition for a Be star not to exhibit shell lines is that the envelope be optically thin in the Hα line, provided the value of β is not too small. According to the central-depth method, shell lines in the Balmer series disappear when τ_α is less than about 100, and the emission components in the lower Balmer lines are sufficiently strong so as to fill up the shell absorptions. These conditions may be fulfilled when the envelope is vertically expanded.

A typical case is the Be-star phase (non-shell) of Pleione which was observed in 1955–1971 (figure 12 of Paper I). In this period the shell lines faded away while emission lines remained sufficiently strong. Let us suppose that Pleione has fulfilled the above condition of shell-line disappearance in this phase. The optical thickness τ_α is given by Hirata & Kogure (1977) as, if we adopt $T = 12000$ K,

$$\tau_\alpha \approx 1.05 \times 10^{-20} N_e^2 \left(\frac{R_2}{R_*}\right) \frac{1}{\overline{W}},$$

where R_2 denotes the outer radius of envelope, $\overline{W}$ the dilution factor at a mid-point of the envelope, and N_e the electron density. If we insert the value of $\tau_\alpha \lesssim 100$ for a typical case of $R_2 \sim 5R_*$, we obtain

$$N_e \lesssim 8 \times 10^9 \text{ cm}^{-3}.$$

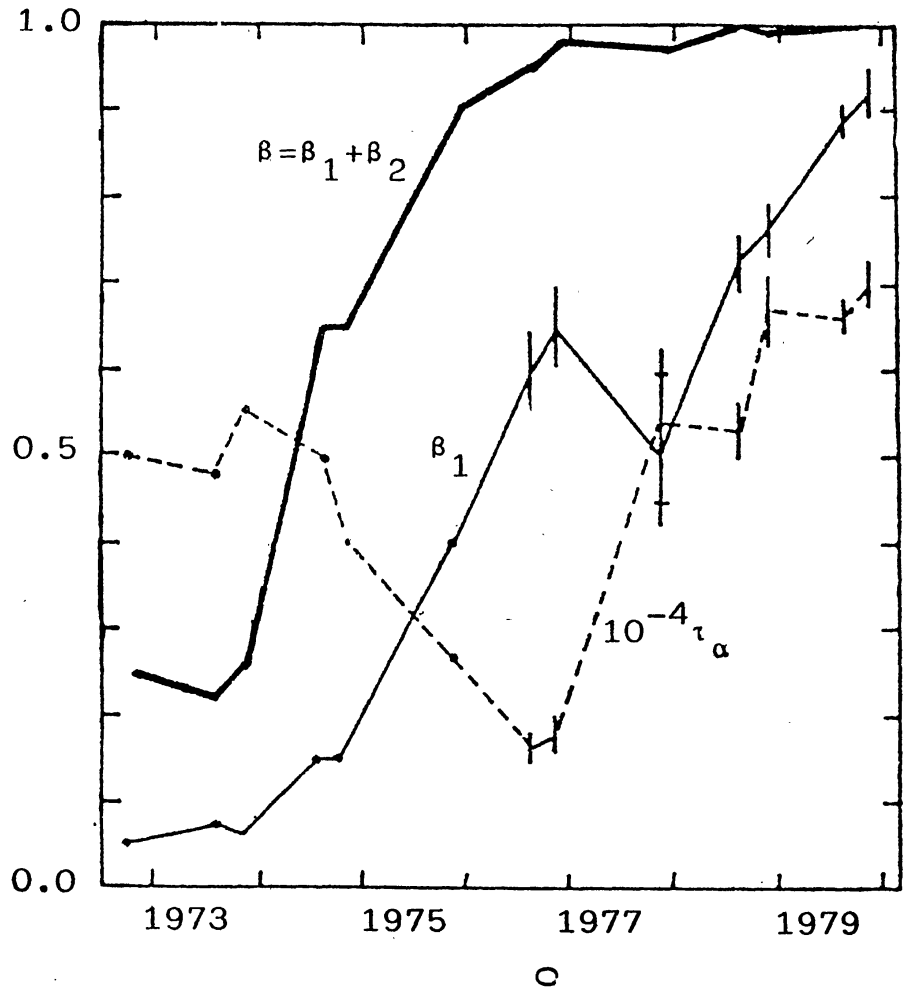

Figure 15. The variation of β and τ_α in the recent shell phase of Pleione (Reproduced from Hirata *et al.* 1982).

This value gives a total mass of $M_{\rm env} \lesssim 2 \times 10^{-10} M_\odot$, if we assume a spherically symmetric envelope. Thus the envelope mass required for the absence of shell lines is slightly higher than or comparable in order of magnitude to that in the early shell phase in 1973–1975 (Hirata & Kogure 1977).

Combining this result with the arguments in figure 11, we can obtain a picture of Pleione's envelope as follows. The Be-star phase in 1955–1971 is possibly characterized by optically thin ($\tau_\alpha \lesssim 100$) but vertically expanded ($H \gg R_*$) envelope. In the shell phase the envelope is optically thick ($\tau_\alpha \sim 4000$) but vertically very concentrated ($H \lesssim R_*$).

According to a long-term monitoring by Hubert-Delplace *et al.* (1979), ordinary Be stars which are rotating faster than $V_* \sin i = 200$ km s^{-1} occasionally disclose shell characteristics in their spectra. In such cases we can suppose that their dense parts of envelope have expanded vertically. For example, if we adopt an intrinsic rotational velocity $V_* = 300$ km s^{-1} for a typical Be star (section 4 of paper I), and if a star with $V_* \sin i = 200$ km s^{-1} showed shell lines, then the envelope of this star should expand vertically covering the stellar photosphere up to about 50° in the star's latitude. Thus the appearance of shell lines in ordinary Be stars yields star candidates with vertically expanded envelopes.

(*iv*) *Emission-line intensities*

The (Hα/Hβ — W_α) diagram considered in section 4.2, allows us to pick up candidate stars having vertically expanded envelopes. That is, if a star is located in figure 8 in the region well below the theoretical curves of $i = 0° \sim 90°$, the envelope of this star should be optically thick ($\tau_{Bc} > 1$) or vertically expanded ($H > 2R_*$) or both. χ Oph, X Per, and π Aqr in some phase may be such condidates in figure 8.

6.3. Disc or ring ?

In section 4.3 we have shown that the disc-like structure is more prevalent than the ring-like in the Be envelopes. The ring-like or detached envelopes, however, may exist as has been often suggested, *e.g.*, by Kogure (1969a) for 11 Cam, and by Jones (1979) for 48 Lib. We consider this problem in this section.

(*i*) *Emission line widths*

The half total-width v_T is a good measure of detachedness, provided rotational broadening among several mechanisms. In this case the inner radius r_1 relative to the stellar radius is given by

$$v_T = v_\phi(1) \sin i . r_1^{-1}, \tag{6-2}$$

where the notation is as defined in section 4.3. If we admit $v_\phi(1) = V_*$, then the width v_T smaller than $V_* \sin i$ suggests the ring-like or detached envelope. Actually, however, emission lines often suffer from broadening by electron scattering, particularly in the lower Balmer members, so that the values of v_T can vary for different lines. In such cases we have to select the lines showing the narrowest width v_T, which are often faint and difficult to measure accurately. Anyway, stars with $v_T < V_* \sin i$ and with sufficiently strong emission intensities are the candidates for detached envelopes. Another comment is that the detachedness found in some lines, say, in hydrogen, does not necessarily mean the detachedness of the envelope itself, because other lines, say He I emission lines, might show non-detached envelope, making a kind of stratification.

(*ii*) *Emission line intensities*

We again consider the (Hα/Hβ — W_α) diagram as given in figure 8. If a star is located well above the theoretical curves calculated for a disc model, then the star should be a candidate for having ring-like envelopes. HD 177648, 1H Cam, and 11 Cam in some epoch, may be such candidates. One may also notice that several stars exhibit marked time variations. Their loci on the diagram should reflect the structural changes of envelopes in geometrical (equatorial and vertical extension and/or detachedness) and in optical properties (values of τ_{Bc}).

In this way figure 8 and similar diagrams calculated for other spectral types provide a good tool of diagnostics of flatness, detachedness, and other structural behaviour. This advantage may be explained by the fact that the value of W_α is determined as an integrated effect from all volume of envelope, *i.e.*, depending on the parameters r_1, r_2, H and τ_{Bc}, whereas the decrement Hα/Hβ is effectively only a function of dilution factor, independent of H and τ_{Bc} as seen in figure 1.

6.4. Axisymmetric or elongated?

The cool envelopes of Be stars are usually supposed to be axisymmetric discs or rings rotating without showing appreciable radial motions. This is a simple picture inferred from the symmetric double-peaked profiles of emission lines. This picture is violated when stars exhibit the V/R variations in their emission line profiles. As has been described in section 8.2 of Paper I, two thirds of Be stars exhibit the V/R variation and a quarter show the quasi-periodic V/R variation. In case of the quasi-periodic V/R variation, the periods are strongly concentrated at about 7 years, and differ from those of E/C variation, the latter being presumably expected to be the activity cycle of Be stars (section 8.2 of Paper I). The statistical nature of V/R variation in case of temporary variation is not yet known. We here confine our discussion to the quasi-periodic V/R variation.

Concerning the origin of the quasi-periodic V/R variation there are in principle two possible ways of interpretation. One is the pulsational motion in axisymmetric envelopes, and the other is the precession of the elongated envelopes. As is well known, purely outflowing envelope forms a P Cyg-type profile. When combined with rotational motion, the resultant profile gives an asymmetry of $V/R < 1$ for outflowing motion, and of $V/R > 1$ for inflowing motion. A simple stellar-wind model based on the outflow motion can only explain the $V/R < 1$ phase, and is not adequate for these variables, since no preferential appearance of $V/R < 1$ phase has been observed (Boyarchuk 1958; Copeland & Heard 1963). The body of emission line shifts bluewards in the $V/R < 1$ phase and redwards in the $V/R > 1$ phase (McLaughlin 1961). McLaughlin (1961) argued that this behaviour cannot be explained by the pulsation model and rejected this hypothesis.

Elliptical ring model was originally suggested by Struve (1931) and supported by McLaughlin (1961) and then developed by Huang (1972, 1973, 1975, 1976) and Kříž (1976a, 1979a, b). The basic idea of this model is that, if gases in an elliptical ring undergo Keplerian motion, the apocentric region of the ring will be more populated by gas than the pericentric region. The long-term V/R variation may be explained by the precession of the elliptic ring. However, the observed profiles and the existence of V/R-variable shell stars support the view that the ring should be wide in its equatorial extension, making elongated discs rather than rings (section 6.2; Kříž 1979b). The variation of shell line width in ζ Tau also supports the elongated disc (Itoh *et al.* 1983). Thus, the elongated disc is the most probable candidate to explain the quasi-periodic V/R variables.

On the formation of elongated discs, there are two ideas; the one is the precession in the binary potential field (Harmanec & Kříž 1976), and the other is the growth of one-arm structure in a Keplerian disc around a single star (Kato 1983). Both seem to explain the period with the order of 7 years. Another mechanism might be of magnetic nature. As seen in section 2.2, of all the magnetohydrodynamical stellar wind is the most promising at present. Then it is not unreasonable to attribute the deformation of envelopes to some effect of magnetic field, though actual process is not yet understood.

In the case of some binary Be stars, the figure of the envelopes is fixed to the binary potential field (stable orbit). Thus, the revolution of envelopes follows the

binary period (ϕ Per, Suzuki 1980; 4 Her, Suzuki 1983, personal communication). It seems that the envelope is fully developed and fills the maximum stable orbit. Marlborough *et al.* (1978), in their stellar wind model for γ Cas, have introduced a third body of the orbital period of about 4 years in order to interpret its V/R variation by elongated disc.

It seems that the elongated disc has been well established in ζ Tau, ϕ Per and 4 Her, all being shell stars belonging to the binary systems. However, it is still uncertain whether all V/R variables have elongated discs or not. For example, behaviour of HD 184279 (B0.5) in spectroscopic and photometric variations seems not to follow the prediction in the frame of elongated disc (Horn *et al.* 1982).

6.5. *Inhomogeneity or multiple components*

The emission-line profiles in the lower Balmer series occasionally reveal triple or even quadruple peaks, as observed, *e.g.* in ζ Tau (Delplace 1970), 27 CMa (Hubert-Delplace *et al.* 1983), or in some stars in the catalogue of Hα profiles by Andrillat & Fehrenbach (1982).

In the shell absorption lines, too, we can see two or even more components in some stars as in EW Lac (Poeckert 1980). Suzuki (1983) has noticed that such multiple components are rather prevalent among Be stars and the radial velocities of absorption components relative to the line centre often exceed several tens km s^{-1}.

These features in emission and shell absorption profiles suggest the existence of inhomogeneity or multiple-component structure in the envelopes of Be stars. No explanation has been given for these features and the accumulation of further observational materials is most desirable.

6.6. *Circular velocity law*

A long-standing but still unsolved problem in the kinematical structure of Be envelopes is the circular velocity law inside the envelopes. This problem is very important not only in the empirical determination of envelope size (section 4.3) but also in the argument of the origin of Be cool envelopes (section 2.2). At present, the tool of diagnostics at our hand is only the line-profile analysis, though unique determination of the circular velocity field is very difficult (section 4.3).

The following three stars present the cases for which the circular velocity law is seemingly well established.

(a) ζ *Oph* (O9.5 V, $V_* \sin i = 320$ km s^{-1}, Slettebak 1982)

This star has shown the emission episodes in 1973–1974 and in 1980 (Ebbets 1981 and references therein). In figure 16 which is constructed from Ebbets (1981) we show the emission profile of the Hα line on 1980 May 28. The photospheric component is subtracted by making use of the profile observed on 1979 September 28 (no emission phase) and a mean profile of blue and red parts is shown because of its symmetry. It is noticed that the wing extends to about 550 km s^{-1}, exceeding the $V_* \sin i$ value. Moreover, the emission peak separation of the He I lines, v_p, is about 400 km s^{-1} (Ebbets 1981). These facts suggest that the inner part of the envelope rotates more rapidly than the star. Discovery of moving features in Hβ and He I lines by Walker *et al.* (1979, 1981) also supports this view, since the

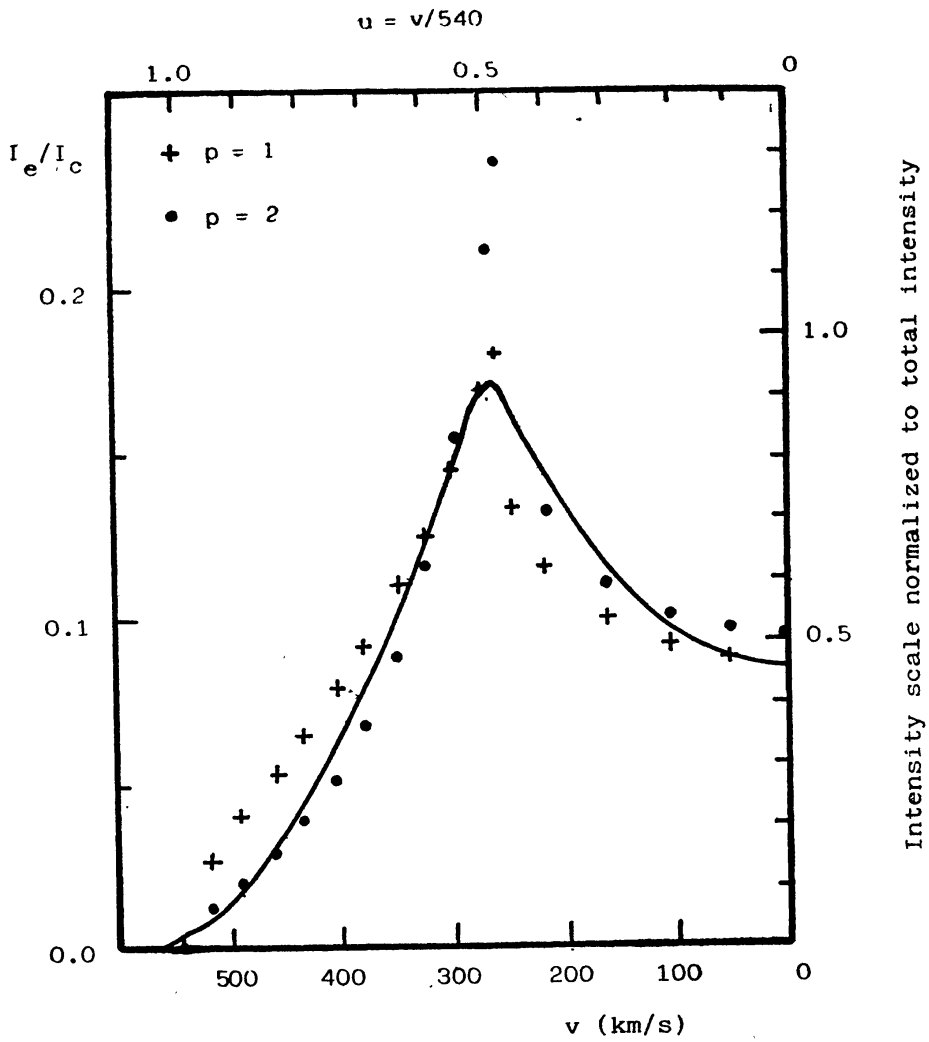

Figure 16. The Hα emission profile (solid line) of ζ Oph on 1980 May 28 (Ebbets 1981) and the function $\Lambda(u)$. The abscissa gives the velocity scale in km s^{-1} (lower side) or in normalized scale $u = v/540$ (upper side). The ordinate denotes the intensity relative to the adjacent continuum (left-hand side) or the normalized intensity to the total intensity (right-hand side). The function $\Lambda(u)$ normalized to the total intensity is shown for cases of $p = 1$ (cross) and $p = 2$ (dot).

V_* sin i value must exceed 500 km s^{-1} if these moving features are supposed to originate in the photosphere (Ebbets 1981; Walker *et al.* 1981). In this way, Ebbets (1981) proposed the Keplerian motion in the envelope, and concluded that the envelope extends from 1 R_* to 4.8 R_*, employing Huang's (1972) disc model.

We note that the circular velocity in the envelope may obey the law of angular momentum conservation even if the innermost part of the envelope rotates with the Keplerian velocity. In figure 16, we also show the function $\Lambda(u)$ defined by equation (4-7). Following the argument of Ebbets (1981) and Walker (1981), we adopt $v_\phi(1) = 660$ km s^{-1} (Keplerian velocity) and $i = 55°$, then $v_\phi(1)$ sin $i = 540$ km s^{-1}. The observed peak separation is $v_p = 260$ km s^{-1}, that is, $u_p = 0.48$. The scale $u = v/[v_\phi(1) \sin i]$ is shown in the upper part of the figure, In the right-hand side of the ordinate, we show the normalized intensity scale so that the total intensity becomes unity in the u-space. The function $\Lambda(u)$ normalized in the same manner

is shown for cases of $p = 1$ (cross) and $p = 2$ (dot). Taking into account the effect of intrinsic broadening function $\psi(u)$ and the occultation of the envelope by the star, we obtain $p \simeq 2$. Then, we have $m \simeq 0$, $r_2 = 2.1$ for $j = 1$, and $m \simeq 1$, $r_2 = 4.3$ for $j = 1/2$. In the case of angular momentum conservation ($j = 1$), we can suppose $m > 0$, because the envelope is formed through the mass loss from the central star and the density should be a decreasing function of r. Thus, we conclude that $j = 1/2$ is preferable.

(b) *ϕ Per* (Bl.5 (V :) e-shell, $V_* \sin i = 400$ km s^{-1}, Slettebak 1982; spectroscopic binary with a period of 127 days)

Suzuki (1980) interpreted the periodic variation of the emission and shell lines in terms of the restricted three-body problem. Later, Poeckert (1981) confirmed the orbital element derived by Suzuki (1980), by the standard radial velocity measurement of the photospheric lines. Though Suzuki (1980) adopted the ring model, his result clearly shows that the motion of the envelope gas is controlled by the potential field in this binary system and suggests Keplerian motion in the inner part near B star.

(c) *Be component of VV Cep* (O8)

The Be envelope is occulted by the M-supergiant primary. The duration of the envelope eclipse was 150 days in 1976, which gives 500 $R_\odot$ for the envelope radius (Kawabata *et al.* 1981). Saijo (1981) has succeeded in the Hα profile fitting out of and during eclipse, and he obtained $v_\phi(r) = 350\, r^{-1/2}$ km s^{-1} and $m = 1.5$ in the notation of section 4.3. Thus, the circular velocity law obeys the Keplerian form. The absolute value of the circular velocity is much smaller than the Keplerian velocity (540 km s^{-1} at $r = 1$). He interpreted this difference in terms of contribution from the radiation pressure (*cf.* Kurucz & Schild 1976). The Be envelope in this system, however, differs from those of the majority of Be stars, because the Be envelope is huge ($\sim 40\, R_*$) and the emission intensity is one or two orders of magnitude stronger than others, if we refer to the Be continuum.

In these cases the Keplerian type of circular velocity has been inferred. However, it is still uncertain whether these results can be generalized to other Be stars or not. The study of correlation in the variation between emission intensity and peak separation in individual stars and the profile analysis, illustrated in the case of ζ Oph, for many Be stars may give some hints to the solution of this problem. From a theoretical point of view, more precise treatment of the non-LTE problem is desirable.

7. Structure and origin of hot regions

General characteristics of hot regions around Be stars have been considered in section 6 of Paper I. In this section we further consider superionization and expansion phenomena detected in the ultraviolet region. One should notice that the superionization is not identical with the hot plasma of $T \sim 10^5$ K (Lamers & Snow 1978), since it can occur in cooler region of $T \sim 10^4$ K by the Auger mechanisms, *i.e.*, by the ionization caused by soft x-rays (Cassinelli & Olson 1979). In the latter case

the source of soft x-rays evidently requires the existence of hot regions somewhere else. Keeping these arguments in mind, we hereafter use the term *hot region* for superionized region.

7.1. Mass loss phenomena in normal B stars

The mass loss phenomena in B and Be stars are considered in some detail in section 7 of Paper I. In this section we emphasize the importance of mass loss processes in normal B stars, since B and Be stars bear close resemblance suggesting common origin.

Table 5 presents mass loss evidence in normal B dwarfs, based on Si IV and C IV lines in the IUE spectra. It is remarkable in table 5 that all the giant stars show mass loss evidence, whereas dwarf stars do not, except the brightest star μ^1 Sco of $M_{bol} \sim -6^m$. There seems no clear relation between mass loss phenomena and stellar rotation, $V_* \sin i$. This result may be compared with that of Doazan *et al.* (1982a) who examined 21 B and Be stars of which 5 are normal B dwarfs and found that 19 out of 21 stars showed mass loss profiles.

Snow (1982) argues that Be stars are almost indistinguishable from normal B stars (including supergiants) in the mass loss phenomena in the ultraviolet domain, with, at most, slight enhancements in Be stars.

Evidently, further studies for larger sample of normal B dwarfs is required for clarifying mass loss and superionization phenomena in normal B dwarfs. And, further comparative studies of B and Be stars are also desirable.

7.2. Geometrical relation

Poeckert (1982) has illustrated four possible types of geometrical relations between hot and cool regions around Be stars. Categorically there are two groups. The one is the one-dimensional arrangement of hot and cool regions such as inner hot region and outer cool region (Doazan *et al.* 1981) or vice versa. The other is the bi-dimensional arrangement consisting of cool equatorial disc and hot expanding region in higher latitude. One may add another possibility of rather

Table 5. Mass loss evidence in normal B stars

Star name	Spectral type	$V_* \sin i^*$ (km s^{-1})	Mass loss evidence**	
			Si IV	C IV
μ^1 Sco	B 1.5 IV	190	o	o
HD 72127 A	B 2 IV	170	×	×
γ Peg	B 2 IV	< 10	×	×
HD 74234	B 2 V	200	×	?
ι Her	B 3 V	10	×	×
τ Her	B 5 IV	30	×	—
D Vel	B 0 III	300	o	o
ν Eri	B 2 III	25	o:	o:
HD 166596	B 3 III	210	o	o
δ Per	B 5 III	200	o	—
ζ Dra	B 5 III	25	Δ	—

*New Slettebak system
**Open circle = mass loss profile (P Cyg, blue winged, or blue shifted)
Cross = symmetric profile
Triangle = suspected mass loss profile

spherical hot expanding region plus cool discrete clouds at the equatorial plane (Gorbatskii 1975).

Hubert-Delplace *et al.* (1983) have examined the behaviour of radial velocities of high-ionization lines in the ultraviolet region and of low-ionization lines in the visible region in ζ Tau and 48 Lib, both of which are *V*/*R*-variable shell stars. They found that the negative velocities in Si IV and C IV resonance lines were kept constant while the lines of low ionization showed sinusoidal velocity variations with positive values. This suggests that the cool and hot regions in these stars should be uncoupled dynamically. Combining this with the fact that the pole-on stars also exhibit mass loss phenomena in the ultraviolet region, Hubert-Delplace *et al.* (1983) support the view of bi-dimensional arrangement.

If we adopt the bi-dimensional structure, the problem will be the relationship between hot and cool regions in their origin and formation. Marlborough *et al.* (1978) suggested that a hot region is formed by the shear instability of the cool equatorial disc. Another view is that the hot region is a hot-expanding wind region, rather spherical and prevailing among normal B stars. If the density becomes high in the equatorial plane for some reason, then, cooling process operates and we obtain a cool equatorial disc. This picture suggests an interpretation for the time variation observed in 59 Cyg (section 8 of Paper I), in which Si IV and C IV lines become enhanced when the Hα emission becomes faint.

7.3. Optical properties

The hot expanding stellar winds around Be stars are complicated by the existence of cool equatorial discs. Moreover, the expanding regions are generally inhomogeneous and often give rise to active phenomena (*e.g.* Doazan *et al.* 1982b; Henrichs 1982). These factors make difficult the modelling of hot expanding regions and we are forced at present to adopt some spherically symmetric wind model for obtaining their global picture.

Snow (1981) has applied Castor & Lamers' (1979) method to Si III and Si IV resonance lines of 22 Be and B stars, and found rather small optical thickness in these lines in case of Be stars as compared to that of supergiants. Snow (1981) has also estimated for 59 Cyg the hydrogen column density $N_H \sim 10^{18}$ cm^{-2} of the region where Si III and Si IV lines are formed. Snow *et al.* (1979) found that sharp Fe III lines in the ultraviolet region generally show small, negative velocities relative to the stars. They concluded that these lines are formed at the bottom of the wind where $N_H \approx 10^{19-21}$ cm^{-2}. Later on, Hubert-Delplace *et al.* (1983) have shown that these sharp Fe III lines are also formed in the extended cool envelopes in case of shell stars. The existence of such doubly ionized iron in cool envelopes is also expected from Fe II emission lines. Hence, if we exclude shell stars from the stars listed by Snow *et al.* (1979), the hydrogen column density in the regions of sharp Fe III line formation is $N_H \sim 10^{19}$ cm^{-2}, much smaller than that of cool equatorial envelopes, $N_H \approx 10^{21-23}$ cm^{-2} (*e.g.* Boyarchuk 1958; Gehrz *et al.* 1974).

These optical properties imply that the gas density in hot expanding winds is much lower than that in cool equatorial envelopes, even if we admit relatively compact regions for the expanding winds. In spite of such a difference, the derived mass loss rates from hot and cool envelopes are comparable, of the order of $10^{-9} \sim 10^{-10}$ $M_\odot$ yr^{-1} (see figure 10 and section 7 of Paper I). The difference in expanding

velocity and/or in source area of gas ejection on the photosphere might account for these features.

Finally we shall make a comment on the argument of Persi *et al.* (1982) on the spherically expanding region as a source of observed infrared excess. Assuming that the infrared excess and ultraviolet resonance lines are formed in the same expanding region, they have derived high mass-loss rates of $5 \times 10^{-7} \sim 8 \times 10^{-6}$ $M_\odot$ yr^{-1} for three x-ray Be stars (HD 245770, γ Cas and X Per). These are several orders of magnitude higher than the figures cited above.

Let us suppose that the infrared radiation is formed in a fully ionized, spherical envelope, expanding with a constant velocity v. Then the mass loss rate is given by

$$\dot{M}(M_\odot/\mathrm{yr}) \geqq 1.8 \times 10^{-6} \left(\frac{R_*}{10R_\odot}\right)^{3/2} \left(\frac{v}{1000}\right) \sqrt{\frac{\alpha}{10^{35}}},$$

where α denotes the volume emission measure defined in section 3.2, $R_\odot$ the solar radius, and v is measured in km s^{-1}. The typical value of α needed for giving observed infrared excess is $10^{35} \sim 10^{36}$ (see section 3.2). Then, so far as we adopt high expanding velocity of $v \sim 1000$ km s^{-1}, high mass-loss rate $\dot{M} \gtrsim 10^{-6}$ $M_\odot$ yr^{-1} is almost inevitable. High temperature of $\sim 10^5$ K does not change the value of α appreciably. It thus becomes clear that the high mass loss rate of Persi *et al.* (1982) is a necessary result of high velocity expansion of envelope.

Actually, the observed infrared excess is well explained by the free-free emission from the cool equatorial envelopes as has been examined in section 3.2. No additional spherical envelope is needed to explain observed infrared excesses. Otherwise, spherically expanding hot region makes little contribution to the infrared excess if we adopt the low mass-loss rate given by Snow (1981).

8. Summary

In Paper I we have considered the general properties of Be stars mainly from the statistical point of view in an attempt to see what the Be stars or the Be stars phenomena are.

As a sequel to Paper I, we have revicwed in this article the formation of spectral lines and continuum, along with the structure of circumstellar envelope of Be stars, particularly of the cool envelopes.

In section 2 theoretical discussion on Be stars as rapid rotators and on envelope dynamics is presented with an emphasis that the magnetohydrodynamical stellar winds would be, at present, a highly promising model of dense and extended cool envelopes of Be stars. The basic properties of the radiation field are also considered from both the static- and moving-envelope approaches.

In sections 3–5, observational features and their theoretical interpretation are extended for the continuous radiation, emission lines, and shell absorption lines.

Section 6 is devoted to the diagnostics of the structure of cool envelopes. Table 6 summarizes spectral features to be used for the diagnosis. Single spectral feature in table 6 is of course insufficient to deduce the structural parameters. However, if we can combine several spectral features, then an overall picture of the envelopes will be obtained for individual stars or for Be stars in general.

In section 7 is reviewed the structure and origin of hot regions. A particular topic is the geometrical relationship of cool and hot regions. Among the

Table 6. Spectral features to be used for the diagnostics of envelope structure

Structure	Spectral feature			
	Emission lines	Shell absorption lines	Continuum and polarization	UV-resonance lines
Gas density, volume	Equivalent	Equivalent width	IR-excess	
Flatness	Intensity (Hα/Hβ—$W\alpha$)	Intensity (Central depth)	Polarization (P%)	Profile
Detachedness	Line width (v_T) Intensity (Hα/Hβ—$W\alpha$)			
Equatorial extension	Peak separation (v_P)	Line width (Half half-width)		
Elongation	Profile (V/R)	Profile (Asymmetry)		
Stratification	Ionization stage	Intensity (Curve of growth) (Central depth)	IR-excess (Type of excess)	Ionization stage
	Line width (v_P, v_T)			Profile
Inhomogeneity	Profile	Profile		Profile
Velocity field	Profile	Profile (Asymmetry) Balmer progression		Profile (Asymmetry)

one-dimensional and bi-dimensional arrangments of both regions, supporting arguments are given for the latter.

In this article, several problems such as line polarization, radio emission, non-thermal processes, have been left out. However, even within the scope of this review, we can observe that, on the one hand, the envelopes of Be stars disclose some definite statistical tendencies against the spectral sequence, the rotational velocity, or some other physical parameters. On the other hand, the envelopes reveal a large variety around their average state. The relationship between individuality and average state is important in the study of Be stars.

Our present knowledge on the structure, origin and activities is very insufficient and fragmentary both for individual stars and for average picture of Be stars. Toward a further understanding, following three steps may be advisable :

(a) Case studies of some representative Be stars, including full diagnostics and sufficient monitoring of variations from a wide spectral range; (b) Non-biased statistical studies of B and Be stars (in, *e.g.*, BS catalogue); and (c) Refinement of model calculations on the theoretical side, to include non-LTE and gasdynamical processes.

Acknowledgements

The authors wish to express their thanks to Dr M. Saito and Mr M. Suzuki for fruitful discussions. Thank are also due to the World Data Centre A for Rockets and Satellites for providing us with the released IUE data. Our indebtedness is also to Miss N. Sakon for typing of the manuscript.

References

Abhyankar, K. D. (1964) *Ap. J.* **140**, 1368.
Allen, D. A. (1973) *M. N. R. A. S.* **161**, 145.
Alvarez, M. & Schuster, W. J. (1982) *Rev. Mex. Astr. Astrof.* **5**, 173.
Andrillat, Y. & Fehrenbach, Ch. (1982) *Astr. Ap. Suppl.* **48**, 91.
Arakelyan, M. A. (1969) *Astrofizika* **5**, 75.
Ballereau, D. (1980) *Astr. Ap. Suppl.* **41**, 305.
Ballereau, D. & Hubert-Delplace, A. M. (1982) *IAU Symp. No. 98*, p. 171.
Barker, P. K. (1982) *IAU Symp. No. 98*, p. 485.
Barker, P. K. & Marlborough, J. M. (1982) *Ap. J.* **254**, 297.
Beeckmans, F. (1976) *Astr. Ap.* **52**, 465.
Beeckmans, F. & Hubert-Delplace, A. M. (1980) *Astr. Ap.* **86**, 72.
Boyarchuk, A. A. (1958) *Sov. Astr. J.* **1**, 192.
Briot, D. (1971, 1977) *Astr. Ap.* **11**, 57; **54**, 599.
Briot, D. (1981a, b) *Astr. Ap.* **103**, 5; **103**, 1.
Briot, D. & Zorec, J. (1981) *Proc. Workshop on Pulsating B Stars*, Nice Observatory, p. 109.
Brown, J. C. & McLean, I. S. (1977) *Astr. Ap.* **57**, 141.
Bruhweiler, F. C., Morgan, T. H. & van der Hucht, K. A. (1982) *Ap. J.* **262**, 675.
Cassinelli, J. P. & Olson, G. L. (1979) *Ap. J.* **229**, 304.
Castor, J. I. & Lamers, H. J. G. L. M. (1979) *Ap. J. Suppl.* **39**, 481.
Collins, G. W. II. & Sonneborn, G. H. (1977) *Ap. J. Suppl.* **34**, 41.
Copeland, J. A. & Heard, J. F. (1963) *Publ. David Dunlap Obs.* **2**, 317.
Coyne, G. V. S. J. (1976) *IAU Symp. No. 70*, p. 233.
Coyne, G. V. S. J. & Kruszewski, A. (1969) *Astr. J.* **74**, 528.
Coyne, G. V. S. J. & McLean, I. S. (1982) *IAU Symp. No. 98*, p. 77.
Dachs, J. *et al.* (1981) *Astr. Ap. Suppl.* **43**, 427.
Delplace, A. M. (1970) *Astr. Ap.* **7**, 459.
Doazan, V. (1965, 1970) *Ann. d'Ap.* **28**, 1; *Astr. Ap.* **8**, 148.
Doazan, V., Franco, M. L., Stalio, R. & Thomas, R. N. (1982a) *IAU Symp. No. 98*, p. 319.
Doazan, V. *et al.* (1982b) *IAU Symp. No. 98*, p. 415.
Doazan, V., Stalio, R. & Thomas, R. N. (1981) *The Universe at Ultraviolet Wavelengths; The First Two Years of IUE* (*ed.* : *R. D. Chapman*) (NASA CP-2171), p. 149.
Ebbets, D. (1981) *Publ. Astr. Soc. Pacific* **93**, 119.
Endal, A. S. (1982) *IAU Symp. No. 98*, p. 299.
Endal, A. S. & Sofia, S. (1979) *Ap. J.* **232**, 531.
Feinstein, A. (1968, 1975) *Zs. f. Ap.* **68**, 29; *Publ. Astr. Soc. Pacific* **87**, 603.
Feinstein, A. (1982) *IAU Symp. No. 98*, p. 235.
Feinstein, A. & Marraco, H. G. (1979) *Astr. J.* **84**, 1713.
Gehrz, R. D., Hacwell, J. A. & Jones, T. W. (1974) *Ap. J.* **191**, 675.
Golay, M. & Mauron, N. (1982) *Astr. Ap. Suppl.* **47**, 547.
Gorbatskii, V. G. (1975) *Sov. Astr. Lett.* **1**, 62.
Harmanec P. (1982) *IAU Symp. No. 98*, p. 279.
Harmanec, P. & Kriz, S. (1976) *IAU Symp. No. 70*, p. 385.
Heap, S. R. (1976) *IAU Symp. No. 70*, p. 165.
Henrichs, H. F. (1982) *IAU Symp. No. 98*, p. 431.
Higurashi, T. & Hirata, R. (1978) *Publ. Astr. Soc. Japan* **30**, 615.
Hirata, R. (1982a, b) *IAU Symp. No. 98*, p. 41; p. 497.
Hirata, R. & Hubert-Delplace, A. M. (1981) *Proc. Workshop on Pulsating B Stars*, Nice Observatory, p. 217.
Hirata, R., Katahira, J. & Jugaku, J. (1982) *IAU Symp. No. 98*, p. 161.
Hirata, R. & Kogure, T. (1976, 1977) *Publ. Astr. Soc. Japan* **28**, 509; **29**, 477.
Hirata, R. & Kogure, T. (1978) *Publ. Astr. Soc. Japan* **30**, 601.
Horn, J. *et al.* (1982) *Bull. Astr. Inst. Czech.* **33**, 308.
Huang, S. S. (1972, 1973) *Ap. J.* **171**, 549; **183**, 541.

Huang, S. S. (1975) *Sky Tel.* **49**, 359.
Huang, S. S. (1976) *Publ. Astr. Soc. Pacific* **88**, 448.
Hubert-Delplace, A. M. & Hubert, H. (1979) *An Atlas of Be Stars*, Meudon Observatory, Paris.
Hubert-Delplace, A. M. *et al.* (1983) *Astr. Ap.* **121**, 174.
Hutchings, J. B. (1970, 1971) *M. N. R. A. S.* **150**, 55; **152**, 109.
Hutchings, J. B. (1976) *Publ. Astr. Soc. Pacific* **88**, 5.
Hutchings, J. B., Nemec, J. M. & Cassidy, J. (1979) *Publ. Astr. Soc. Pacific* **91**, 313.
Jaschek, M., Hubert-Delplace, A. M., Hubert, H. & Jaschek, C. (1980) *Astr. Ap. Suppl.* **42**, 103.
Itoh, S., Hirata, R. & Hubert-Delplace A. M. (1983) in preparation.
Jones, T. J. (1979) *Ap. J.* **228**, 787.
Kato, S. (1983) *Publ. Astr. Soc. Japan* **35**, 249.
Kawabata, S., Saijo, K., Sato, H. & Saito, M. (1981) *Publ. Astr. Soc. Japan* **33**, 177.
Kodaira, K. & Hoekstra, R. (1979) *Astr. Ap.* **78**, 292.
Kogure, T. (1959a, b) *Publ. Astr. Soc. Japan* **11**, 127; 278.
Kogure, T. (1961, 1967) *Publ. Astr. Soc. Japan* **13**, 335; **19**, 30.
Kogure, T. (1969a) *Astr. Ap.* **1**, 253.
Kogure, T. (1969b, 1975) *Publ. Astr. Soc. Japan* **21**, 71; **27**, 165.
Kogure, T. & Hirata, R. (1982) *Bull. Astr. Soc. India* **10**, 281 (Paper I).
Kogure, T., Hirata R. & Asada, Y. (1978) *Publ. Astr. Soc. Japan* **30**, 385.
Kříž, S. (1973, 1976a) *Bull. Astr. Inst. Czech.* **25**, 143; **27**, 321.
Kříž, S. (1976b) *IAU Symp. No. 70*, p. 323.
Kříž, S. (1979a, b) *Bull. Astr. Inst. Czech.* **30**, 83; 93
Kříž, S. (1982) *Bull. Astr. Inst. Czech.* **33**, 302.
Kupo, I. D. (1969) *Trud. Ap. Inst. AN Kazav. SSR* **14**, 32.
Kurucz, R. L. (1979) *Ap. J. Suppl.* **40**, 1.
Kurucz, R. L. & Schild, R. E. (1976) *IAU Symp. No. 70*, p. 377.
Lacoarret, M. (1965) *Ann. d'Ap.* **28**, 321.
Lamers, H. J. G. L. M. & Snow, T. P. (1978) *Ap. J.* **219**, 504.
Landstreet, J. D. (1980) *Astr. J.* **85**, 611.
Limber, D. N. (1964, 1967) *Ap. J.* **140**, 1391; **148**, 141.
Limber, D. N. (1974) *Ap. J.* **192**, 429.
Limber, D. N. & Marlborough, J. M. (1968) *Ap. J.* **152**, 181.
Marlborough, J. M. (1969, 1970) *Ap. J.* **156**, 135; **159** 575.
Marlborough, J. M. (1976, 1982) *IAU Symp. No. 70*, p. 335; *IAU Symp No. 98*, p. 361.
Marlborough, J. M. & Cowley, A. P. (1974) *Ap. J.* **187**, 99.
Marlborough, J. M. & Gredley, P. R. (1972) *Ap. J.* **178**, 477.
Marlborough, J. M., Snow, T. P. & Slettebak, A. (1978) *Ap. J.* **224**, 157.
Marlborough, J. M. & Zamir, M. (1975) *Ap. J.* **195**, 145.
McLaughlin, D. B. (1961) *J. R. Astr. Soc. Canada* **55**, 73.
McLean, I. S. (1979) *M. N. R. A. S.* **186**, 265.
McLean, I. S. & Brown, J. C. (1978) *Astr. Ap.* **69**, 291.
Mendoza, E. E. (1982) *IAU Symp. No. 98*, p. 3.
Merrill, P. W. & Sanford, R. F. (1944) *Ap. J.* **100**, 14.
Metz, K. (1982) *IAU Symp. No. 98*, p. 95.
Mihalas, D. (1979) *M. N. R. A. S.* **189**, 671.
Miyamoto, S. (1949) *Jap. J. Astr.* **1**, 17.
Miyamoto, S. (1952a, b) *Publ. Astr. Soc. Japan* **4**, 1; 28.
Morozov, V. N. (1973) *Astrofizika* **9**, 387.
Nerney, S. (1980) *Ap. J.* **242**, 723.
Neto, A. D. & Pacheco, J. A. de Freitas (1982) *M. N. R. A. S.* **198**, 659.
Nordh, H. L. & Olofsson, S. G. (1977) *Astr. Ap.* **56**, 117.
Özemre, K. (1967) *Ann. d'Ap.* **30**, 495.
Peraiah, A. (1982) *J. Ap. Astr.* **3**, 297.

Persi, P., Ferrari-Toniolo, M. & Grasdalen, G. L. (1982) *IAU Symp. No. 98*, p. 247.
Poeckert, R. (1980) *Publ. Dominion Ap. Obs. Victoria* **15**, 357.
Poeckert, R. (1981) *Publ. Astr. Soc. Pacific* **93**, 297.
Poeckert, R. (1982) *IAU Symp. No. 98*, p. 453.
Poeckert, R., Bastien, P. & Landstreet, J. D. (1979) *Astr. J.* **84**, 812.
Poeckert, R. & Marlborough, J. M. (1976, 1977) *Ap. J.* **206**, 182; **218**, 220.
Poeckert, R. & Marlborough, J. M. (1978a,b) *Ap. J.* **220**, 940; *Ap. J. Suppl.* **38**, 229.
Poeckert, T. & Marlborough, J. M. (1979) *Ap. J.* **233**, 259.
Polidan, R. S. (1976) *IAU Symp. No. 70*, p. 401.
Polidan, R. S. & Peters, G. J. (1976) *IAU Symp. No. 70*, p. 59.
Pottasch, S. R. (1961) *Ann. d'Ap.* **24**, 159.
Ruusalepp, M. (1982) *IAU Symp. No. 98*, p. 303.
Sackmann, I. J. & Anand, S. P. S. (1970) *Ap. J.* **162**, 105.
Saijo, K. (1981) *Publ. Astr. Soc. Japan* **33**, 351.
Saito, M. (1974) *Publ. Astr. Soc. Japan* **26**, 103.
Schild, R. E. (1976) *IAU Symp. No. 70*, p. 107.
Scholz, G. (1981) *Bull. Astr. Inst. Czech.* **32**, 56.
Slettebak, A. (1976) *IAU Symp. No. 70*, p. 123.
Slettebak, A. (1982) *Ap. J. Suppl.* **50**, 55.
Slettebak, A., Kuzma, T. J. & Collins, G. W. II (1980) *Ap. J.* **242**, 171.
Snow, T. P. (1981) *Ap. J.* **251**, 139.
Snow, T. P. (1982) *Advances in Ultraviolet Astronomy : Four Years of IUE Research (eds : Y. Kondo, J. M. Mead, R. C. Chapman)* (NASA CP-2238), p. 61.
Snow, T. P., Peters, G. J. & Mathieu, R. D. (1979) *Ap. J. Suppl.* **39**, 359.
Sobolev, V. V. (1947) *Dvizhushchiesya Obolochki Zvezd* [English translation : *Moving Envelopes of Stars, translated by S. Gaposchkin*, 1960 (Harvard Univ. Press)].
Sobolev, V. V. (1960) *Sov. Astr. J.* **3**, 735.
Sonneborn, G. (1982) *IAU Symp. No. 98*, p. 493.
Sonneborn, G. & Collins, G. W. II (1977) *Ap. J.* **213**, 787.
Struve, O. (1931) *Ap. J.* **73**, 94.
Suzuki, M. (1980) *Publ. Astr. Soc. Japan* **32**, 331.
Underhill, A. B. (1949) *Ap. J.* **110**, 166.
Underhill, A. B. (1952, 1954) *Publ. Dominion Ap. Obs. Victoria* **9**, 139; 363.
Von Zeipel, H. (1924) *M. N. R. A. S.* **84**, 665.
Walker, G. A. H., Yang, S. & Fahlman, G. G. (1979) *Ap. J.* **233**, 199.
Walker, G. A. H., Yang, S. & Fahlman, G. G. (1981) *Proc. Workshop on Pulsating B Stars*, Nice Observatory, p. 261.
Weber, E. J. & Davis, L. (1967) *Ap. J.* **148**, 217.
Wellman, P. (1952a, b) *Zs. Ap.* **30**, 71; 88
Wellman, P. (1952c, 1955) *Zs. Ap.* **30**, 96; *Vistas Astr.* **1**, 303.